SIMULATION, FABRICATION, AND CHARACTERIZATION OF

SEMICONDUCTOR LASERS

by

Banaful Paul

APPROVED BY SUPERVISORY COMMITTEE:

____

Dr. Ann Catrina Coleman, Chair

____

Dr. James J. Coleman

____

Dr. Qing Gu

This thesis is dedicated to

my parents and my wife, Pipasha

SIMULATION, FABRICATION, AND CHARACTERIZATION OF

SEMICONDUCTOR LASERS

by

BANAFUL PAUL

THESIS

Presented to the Faculty of

The University of Texas at Dallas

in Partial Fulfillment

of the Requirements

for the Degree of

MASTER OF SCIENCE IN

ELECTRICAL ENGINEERING

THE UNIVERSITY OF TEXAS AT DALLAS

August 2018

ACKNOWLEDGMENTS

I would like to express my sincere gratitude to my supervisor, Professor Ann Catrina Coleman, for her continuous support, encouragement, and guidance throughout my master's research here at The University of Texas at Dallas. The invaluable research experience I gathered here has been made possible because of her kind guidance and inspiration. There were times when I faced difficulties both in research and my personal life. The support I received from Professor Catrina Coleman at those moments truly reminds me how fortunate I am to have a mentor like her.

I am also thankful to Professor James Coleman and Professor Qing Gu for being a part of my thesis committee, and also for their indispensable support and advice regarding my research works. I want to thank Professor Andrea Fumagalli for allowing me to work with his research team, which helped me to extend my research experience beyond my own research concentration. I consider myself lucky to have come across a lot of great faculty members here, under whom I have taken a lot of graduate courses. I am thankful to all of them. I am grateful to Professor Lawrence Overzet and to Professor Lakshman Tamil for their support when I needed it the most.

Thanks to Jianfei Chen for being my group mate and helping me out to set up several instruments. I am thankful to Abouzar Gharajeh, Jiyoung Moon, Xi Li, Zhitong Li and Farhat Abbas from Dr. Qing Gu's group for their support while working in the lab.

I will always remember the technical support I obtained from John and also the administrative support of Melissa Maxey. I am thankful to all the staff of the cleanroom, particularly to Roger Robbins, Gordon Pollack and John Goodnight for their cordial support.

Finally, I want to express my gratitude and love for my family members for whom I am who I am today. I am grateful to the Almighty for blessing me with this lovely family who supported me in every sphere of my life and also for everything in my life.

SIMULATION, FABRICATION, AND CHARACTERIZATION OF

SEMICONDUCTOR LASERS

Banaful Paul, MS
The University of Texas at Dallas, 2018

Supervising Professor: Dr. Ann Catrina Coleman, Chair

Semiconductor lasers are very important in today's world, considering their applications in communication, medical, spectroscopy and also in our daily lives.This thesis discusses three different types of laser: broad area, ridge waveguide and mode locking laser. Broad area laser (BAL) is the simplest to fabricate among these three lasers which is utilized for characterization of the material, whereas the ridge waveguide laser confines light within the fabricated ridge. The mode lock laser is similar to ridge waveguide laser except that the contact metal is divided into two sections. One section acts as the gain medium and the other section works as the saturable absorber thus providing passive modelocking. The measured threshold current for BAL is around 140 mA whereas it is 26 mA and 36 mA for ridge waveguide and passively mode locked laser respectively for 1 mm cavity length. The threshold current density is also calculated 139.91 A/cm^2 for infinite cavity length. Optical spectrum measurement showed wavelength around 892 nm to 898 nm for all the lasers. External differential quantum efficiency is measured for different cavity lengths from which internal quantum efficiency is found 85.5% and also internal loss 5.85 cm^{-1}. Finally, the characteristic temperature for the diode laser is found 208.3 ^0C. It is also shown that the slope decreases and the threshold current increases for increasing reverse bias for the passively mode locked laser.

TABLE OF CONTENTS

LIST OF FIGURES

LIST OF TABLES

CHAPTER 1

INTRODUCTION

Starting with the advent of the semiconductor laser, it has always been considered as a very reliable, compact, efficient and low-cost optical source. The idea behind the lasing action was first described by Albert Einstein when he postulated the idea of stimulated emission. However, the diode lasers we are now familiar with was described by Basov (Basov et al., 1961) and later by Bernard and Duraffourg (1961) and Dumke (1962) (Blood, 2015). Semiconductor lasers consist of p-n junctions which are forward biased. This biasing causes electron-hole recombination at the junction which emits light and the cleaved facets provide the optical feedback necessary to maintain the optical gain (Agrawal and Dutta, 2013). Most of the diode lasers were GaAs at that time which is known as direct bandgap material. For the direct bandgap materials, the minimum of the conduction band coincides with the maximum of the valence band when plotted against the propagation constant or wave vector, k. Due to this, electrons from the conduction band can make a transition to an empty valence band without changing any k value (Streetman and Banerjee, 2016). The energy given off by the electron is emitted as a photon with wavelength λ related to the direct band gap energy, E_g by the following equation:

$$E_g = hf = \frac{hc}{\lambda} \tag{1.1}$$

$$or, \lambda(\mu m) = \frac{1.24}{E_g(ev)} \tag{1.2}$$

However, things are different for indirect bandgap material where the minimum of the conduction band doesn't coincide with the maximum of the valence band. Therefore, an electron cannot make a transition to the empty valence band without changing the wave vector k. Changing of wave vector k requires phonon assistance which makes the transition less probable compared to direct bandgap material. Therefore, the light output from indirect bandgap material like Si is very improbable.

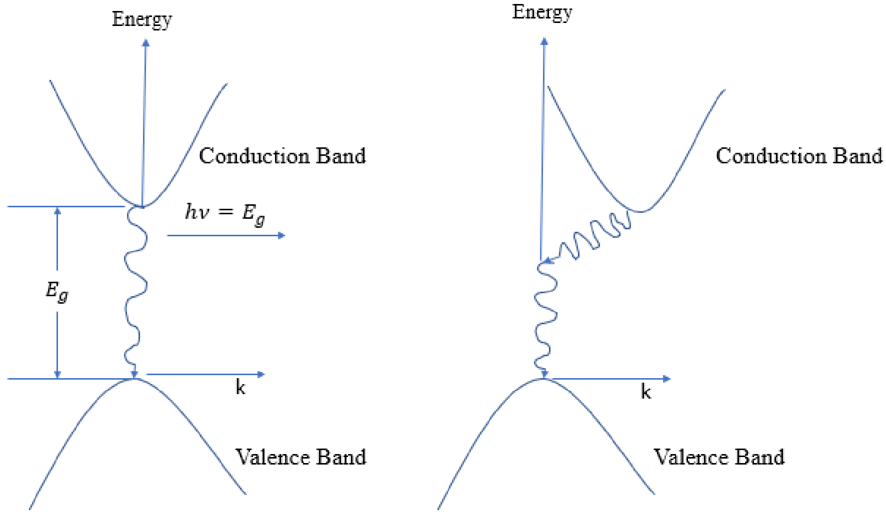

Figure 1.1: Direct (left) and indirect (right) transition of electrons in semiconductor

There are three types of optical process that can occur in a semiconductor as shown in Figure 1.2:

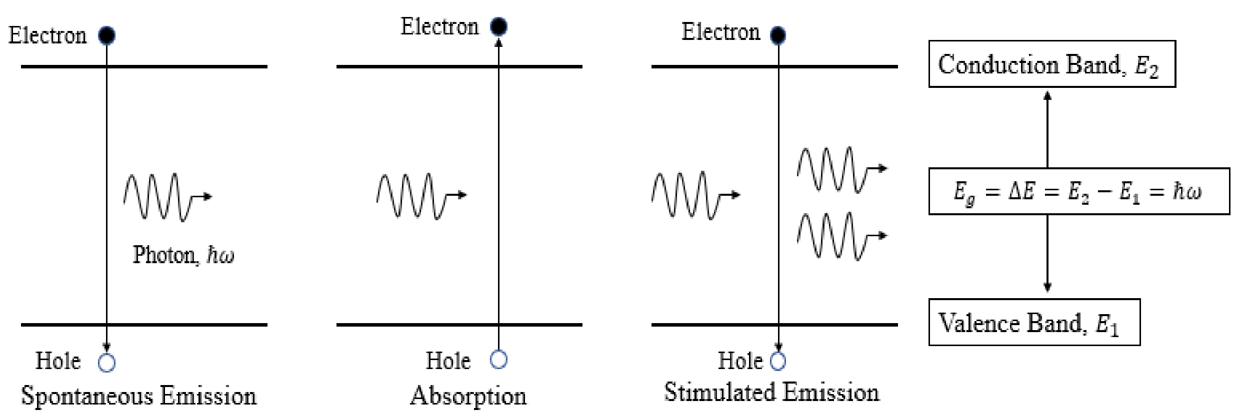

Figure 1.2: Different band to band optical processes in semiconductors

The first process is called spontaneous emission. Here, an electron makes a transition from the conduction band to the valence band and emits a photon in this process. The emitted photon is random in phase and direction also known as incoherent radiation. Since this process depends on the availability of electrons and holes in the conduction band and valence band respectively, the transition probability is a product of electron and hole density.

Considering, conduction band energy as E_2 and valence band energy as E_1, the emitted photon energy is, $E_2 - E_1 = \hbar\omega = E_g$.

The next process is the opposite of spontaneous emission and is known as absorption. After absorbing a photon, an electron-hole pair is generated. If the photon energy is equal to E_g, after absorbing this energy the electron will jump to energy level E_2 from E_1. This process depends on the density of occupied states by electrons at energy level E_1, the unoccupied density of states at energy level E_2 and the photon density with energy $\hbar\omega$ (Diehl and Diehl, 2000).

The final process is known as stimulated emission. If a photon with energy $\hbar\omega$ hits an electron at energy level E_2, a second photon with the same phase, direction and wavelength will be emitted thus amplifying the incoming light. This is the principle on which Lasers are based and thus justify the acronym Light Amplification by Stimulated Emission of Radiation (LASER).

Population inversion is necessary for achieving optical gain in the laser. This means the population of the conduction and valence bands must be inverted. At thermal equilibrium, this is not the case and therefore special measures are taken for achieving population inversion. In the simplest form of semiconductor laser, a p-n junction is forward biased and electron-hole recombination occurs at the junction and the light is emitted. However, due to very small gain volume, the threshold current density of these lasers was very high ($J_{th} \geqslant 50\, KA/cm^2$) (Agrawal and Dutta, 2013) due to which continuous operation of these lasers at room temperature was not possible. The other problems with the pn diode as a laser is the lack of confinements of the carriers - they diffuse several microns. Also the photons are only weakly guided. To overcome this problem, it was suggested that if a lower bandgap material can be inserted in between two high bandgap materials, population inversion will be very easy to achieve and therefore the threshold current will be reduced significantly (Hall et al., 1962) (Nathan et al., 1962). Due to higher bandgap materials, the carriers will be trapped within the middle layer. Also, since higher bandgap material has a lower refractive index, it will also provide optical mode confinement close to the active region which significantly reduces the internal loss (Nelson and Kressel, 1969). This structure is known as heterostructure laser opposed to the previous homojunction laser. Depending on whether the active region is surrounded by single or double higher bandgap material, it is called single or double heterostructure (Agrawal and Dutta, 2013). Even though the idea of reducing the threshold current of the diode laser was very simple, there was one issue which seemed very daunting. Since two different semiconductors were required to be grown on top of each other, matching of lattice constant was very important. If the unmatched layers were relaxed, there will be defects in the junction which will degrade the laser quality. In 1969, GaAs double heterostructure lasers achieved low threshold current density of $J_{th} = 5\,KA/cm^2$ which was further reduced to $J_{th} = .5\,KA/cm^2$ by AlGaAs layers and very thin active layers ($.1\ \mu$). (Agrawal and Dutta, 2013) (Alferov, 1969) (Ettenberg, 1975). To further reduce the threshold current, quantum well layers are utilized which make the energy levels discrete. Quantum well made it possible to grow materials with modest strain due to lattice mismatch. In fact, the strain provided few advantages compared to conventional ones such as enabling modification of band structure to increase the coverage of wavelength and also to improve performance of the devices. (Blood, 2015)

Once the light is generated inside the active layers, it is confined within the vicinity of the active layer due to total internal reflection. Therefore, if μ_1 an μ_2 are the refractive indices of the cladding and the core layers respectively, the generated light will be reflected back whenever the incident angle hits with an angle greater than the critical angle, θ_c

$$\theta_c = sin^{-1}\frac{\mu_1}{\mu_2} \tag{1.3}$$

Now, a threshold condition is required to be figured out for stable operation of a diode laser.

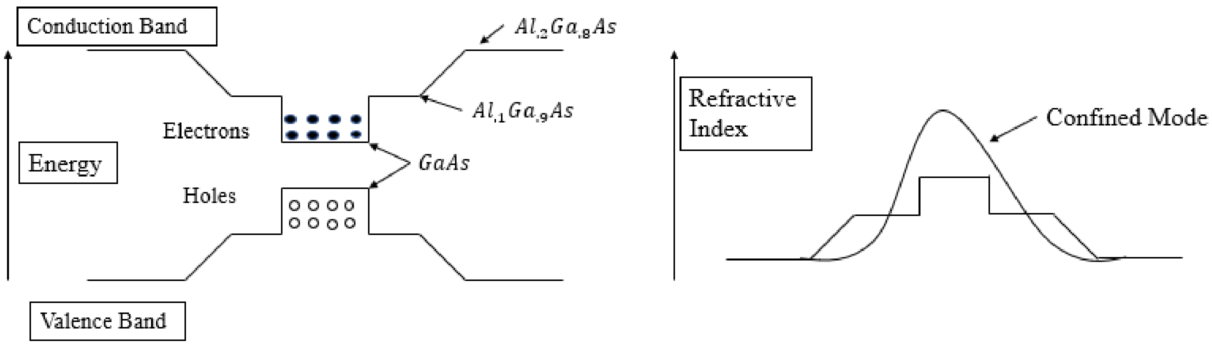

Figure 1.3: Confinement of the charge carriers and the optical mode in the active region of a double hetero-structure

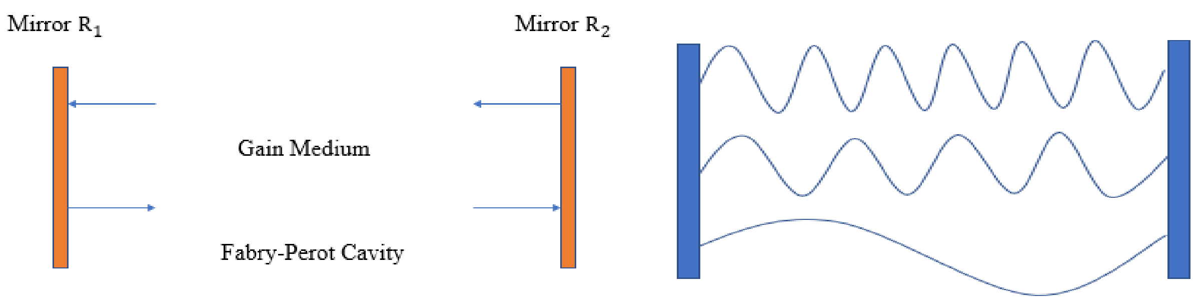

Figure 1.4: Fabry-Perot Cavity (left) and multiple longitudinal modes within the cavity (right)

The threshold condition is given by,

$$\Gamma g = \alpha_m + \alpha_{int} \tag{1.4}$$

where, Γ is the confinement factor which takes into account the reduced gain due to spreading of the optical mode outside of the active region, g is the net gain, α_{int} is the loss that considers losses due to scattering at the heterojunction and also loss due to free carrier absorption and α_m is the loss due to mirrors at the two facets of the laser. If R1 and R2 are the mirror reflectivities and L is the cavity length, the mirror loss is given by

$$\alpha_m = \frac{1}{2L} * ln\frac{1}{R_1R_2} \tag{1.5}$$

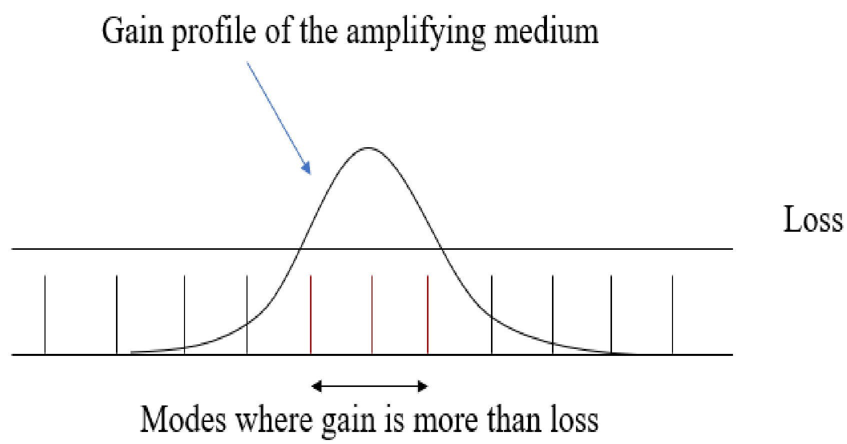

Figure 1.5: Lasing longitudinal modes

Now, allowed modes within the optical cavity are the ones for which the length of the cavity is equal to the integral of the half wavelength as shown in the Figure 1.4.

$$L = \frac{m\lambda}{2n} \tag{1.6}$$

where m is the number of modes and n is the refractive index. Considering two immediate modes, the longitudinal mode spacing in frequency is found as

$$\Delta\nu = \frac{c}{2nL} \tag{1.7}$$

where c is the speed of light. The modes which are within the gain profile and have gain more than loss are the ones which will survive. It can be seen from the Figure 1.5

In general, there is no fixed relation concerning phase among these modes. Therefore, the intensity variation of these modes will be random in nature. Mode locking is a pulse generation technique in which a fixed phase relation is introduced among these longitudinal modes (Pusino, 2013). Due to this fixed phase relation, there will be a sequence of short optical pulses in the output the diode lasers. Depending on the way of introducing this fixed phase relation, the mode locking can be classified as active, passive or hybrid. In active mode locking, an external gain modulation is applied to the diode laser at the cavity

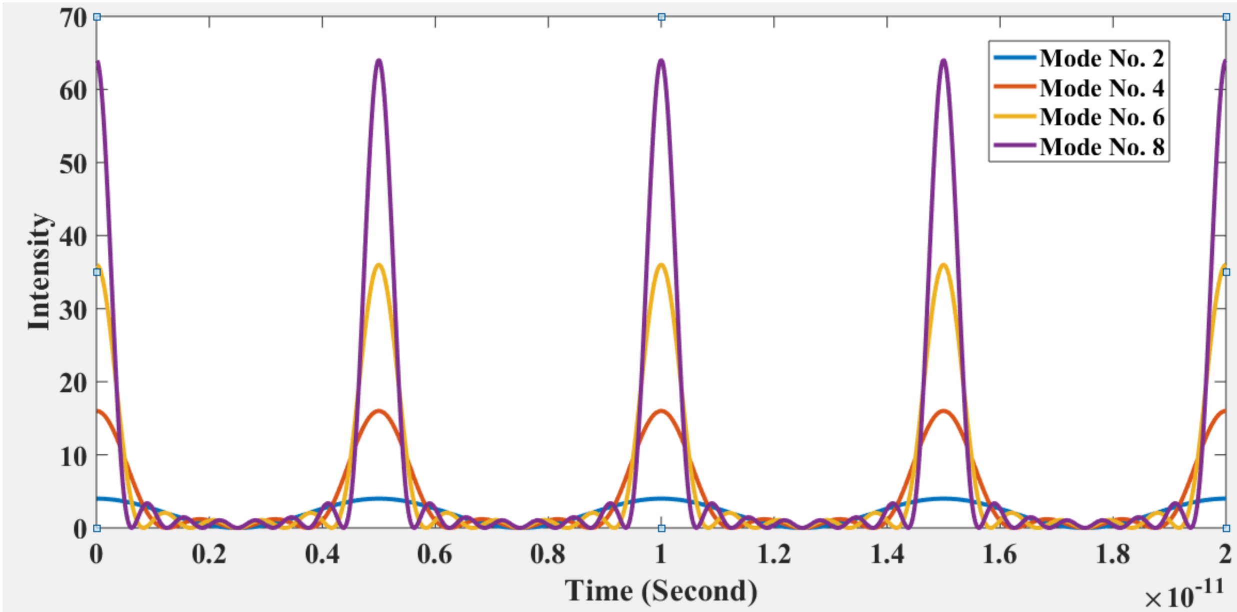

Figure 1.6: Dependence of pulse width and electric field intensity on the number of locked longitudinal modes

round trip frequency (Pusino, 2013). Since, the modulation frequency is dependent on the external circuit, this technique cannot provide a very high repetition rate. For passive mode locking, a non-linear element like saturable absorber is placed within the cavity which locks the longitudinal modes (Pusino, 2013) (Camacho, 1998). In hybrid technique, both active element and the saturable absorbers are used.

It can be seen from the Figure 1.6 that with increasing the number of modes the pulses become shorter and the intensity increases (Pusino, 2013). To achieve mode locking in diode laser, current is applied to the gain section and a reverse bias is applied to the absorber section where there is an isolation between the gain and the absorber section (Hou et al., 2011) (Marsh and Hou, 2017). It is the interplay between these two sections which generates and shorten the pulses. Among the random fluctuating pulses, the ones with the low intensity will be absorbed by the absorber section (Yanson et al., 2002) (Pusino et al., 2014). The high intensity ones will saturate the absorber and will continue to grow with each round trip within the optical cavity. It is required that the absorber section should recover faster than the gain section for stable pulse formation (Pusino, 2013) (Martins-Filho et al., 1995) and the application of reverse bias improves the recovery time of the absorber section.

In this thesis, different types of semiconductor laser structures are investigated. Chapter 2 describes the simulation performed before starting the fabrication to figure out the required ridge height. FIMMWAVE software is used to perform the simulations. Chapter 3 explains in details about the fabrication process for broad area laser, ridge waveguide laser and 2 section laser. Chapter 4 discusses about the setup of the characterization facility in the lab. Chapter 5 shows the results from the characterization of these lasers followed by the conclusion in Chapter 6 which also includes the future work direction.

CHAPTER 2

SIMULATION

There are a lot of parameters that are required to be figured out before starting of the fabrication of the diode laser. Ridge height and ridge width are two of these. For simulating diode laser structures, FIMMWAVE software is utilized here. This software can simulate different 2-D and 3-D structures using a semi-analytical method like Film Mode Matching (FMM) solver or numerical methods like Finite Difference Method (FDM) and Finite Element Method (FEM). We utilized this software for defining the ridge waveguide structure using the epi-layers supplied by the material provider. One of the important things to design is to find the right condition for the diode lasers to lase in the fundamental spatial mode. This chapter will aim to define this design issue. We received our material for diode laser from IQE. The material structure is shown in Table 2.1

The first step is to define the layers as shown in the material data. While designing, it is important to apply few simplifications, which will significantly reduce the simulation time without having any impact on the results. One of the things is to skip the substrate from the epi-layers, which is a very thick layer. Since the active region of the material is far away from the substrate, the substrate will not see the modes. The same concept is also applicable to the top GaAs layer, which acts as a contact layer with high doping concentration. Skipping these layers will reduce the simulation domain and speed up the simulation process. For defining the epi-layers, we need to input the refractive index of the materials with different Aluminum (Al) and Gallium (Ga) composition. For this, a semi-empirical method shown by Martin A. Afromowitz (Afromowitz, 1974) to calculate the refractive index of $Ga_{1-x}Al_xAs$ at energies below the band edge is used. The refractive index profile is shown in Figure 2.1:

The material will operate at a wavelength of 799 nm. In addition, we will only consider TE mode and will ignore TM mode, as output from the quantum well diode lasers mostly emits light with TE mode. We are interested to obtain only the fundamental mode. Ridge

Table 2.1: Material data from IQE

Layer	Material	Mole Fraction (x)	Thickness (μm)	Dopant	Type	CV Level
12	GaAs		0.1500	Zinc	P	>2.00e19
11	Al(x)GaAs	0.550 to 0.050	0.0500	Zinc	P	>2.00e18
10	Al(x)GaAs	0.550	1.1000	Zinc	P	=7.00e17
9	Al(x)GaAs	0.550	0.1000	Zinc	P	=2.00e17
8	Al(x)GaAs	0.250 to 0.550	0.1500	undoped	U/D	
7	Al(x)GaAs	0.250	0.0050	undoped	U/D	
6	GaAs		0.0040	undoped	U/D	
5	Al(x)GaAs	0.250	0.0050	undoped	U/D	
4	Al(x)GaAs	0.550 to 0.250	0.1500	Silicon	N	=1e18 to 1e17
3	Al(x)GaAs	0.550	1.2000	Silicon	N	=1.00e18
2	Al(x)GaAs	0.050 to 0.550	0.0500	Silicon	N	=1.00e18
1	GaAs		0.5000	Silicon	N	=2.00e18

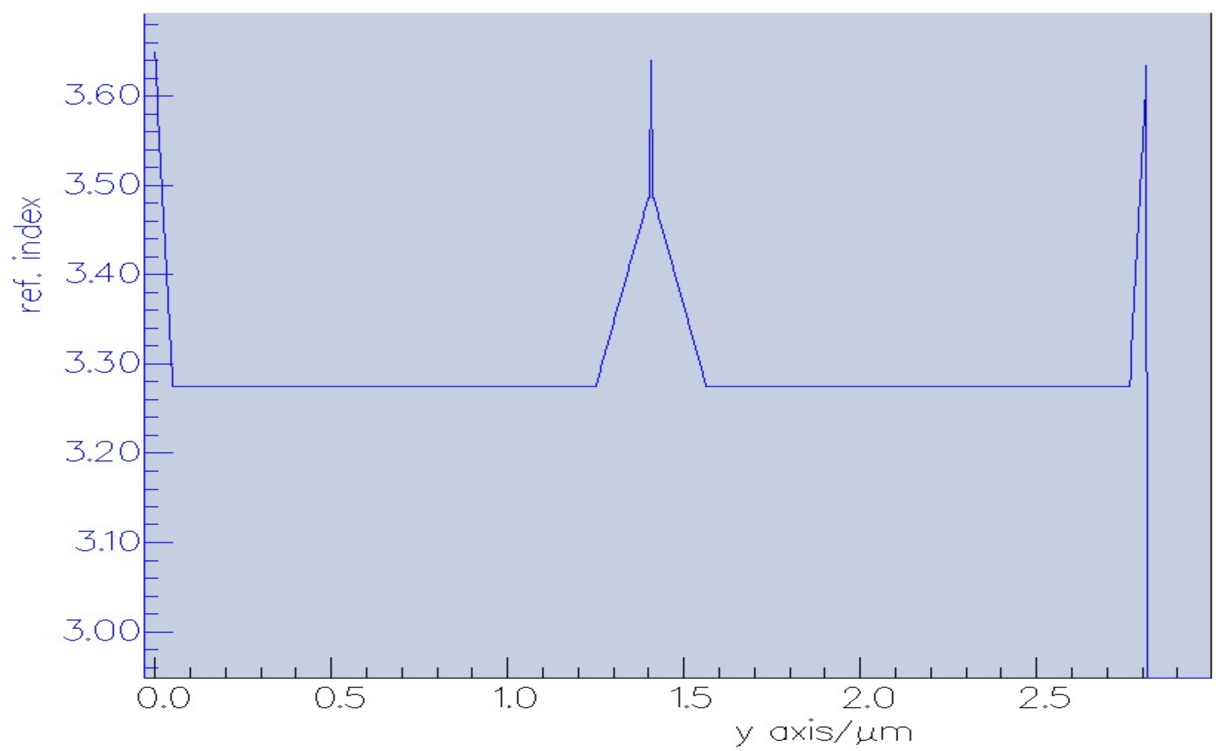

Figure 2.1: Refractive index profile of the material

width and ridge height determine whether there will be fundamental mode or higher order modes. It is found that ridge width between 3 μm to 5 μm is an essential condition for obtaining fundamental mode. However, it also depends on the ridge height. Therefore, in this simulation, we will vary the ridge height to see the impact of height on different modes for different ridge width. As the ridge height is increased, the effective refractive index difference between the ridge and the etched region increases. This will favor confinement of higher order modes, which will finally induce kinks in the output light for lower current due to switching from one mode to another. (Qiu et al., 2004) We will consider the side loss to determine whether a mode will propagate or radiate away from the waveguide. If the side loss is zero or very small, it means the mode will propagate. Modes with high side loss will eventually radiate away from the waveguide. Therefore, the design goal will be to have a lower loss for fundamental mode and higher loss for higher order modes.

2.1 Ridge Width 2.5 μm

For ridge width of 2.5 μm, the height of the ridge is varied from 1.1 μm to 1.4 μm. The corresponding change in the mode profiles of fundamental mode and the higher order modes is shown in Figure 2.2

It can be seen from Figure 2.2 that with the increase of the ridge depth, the confinement of the modes within the ridge increases significantly. This reduces the corresponding side loss associated with all the modes (Qiu et al., 2005). Therefore a depth is needed to be found where the fundamental mode will be lossless but the higher order modes will have loss. This will make sure that the threshold current for the higher order modes will be higher.

2.2 Ridge Width 3 μm

The same simulation is performed for ridge width 3 μm with ridge height varying from 1.1 μm to 1.4 μm. The output is shown in Figure 2.3

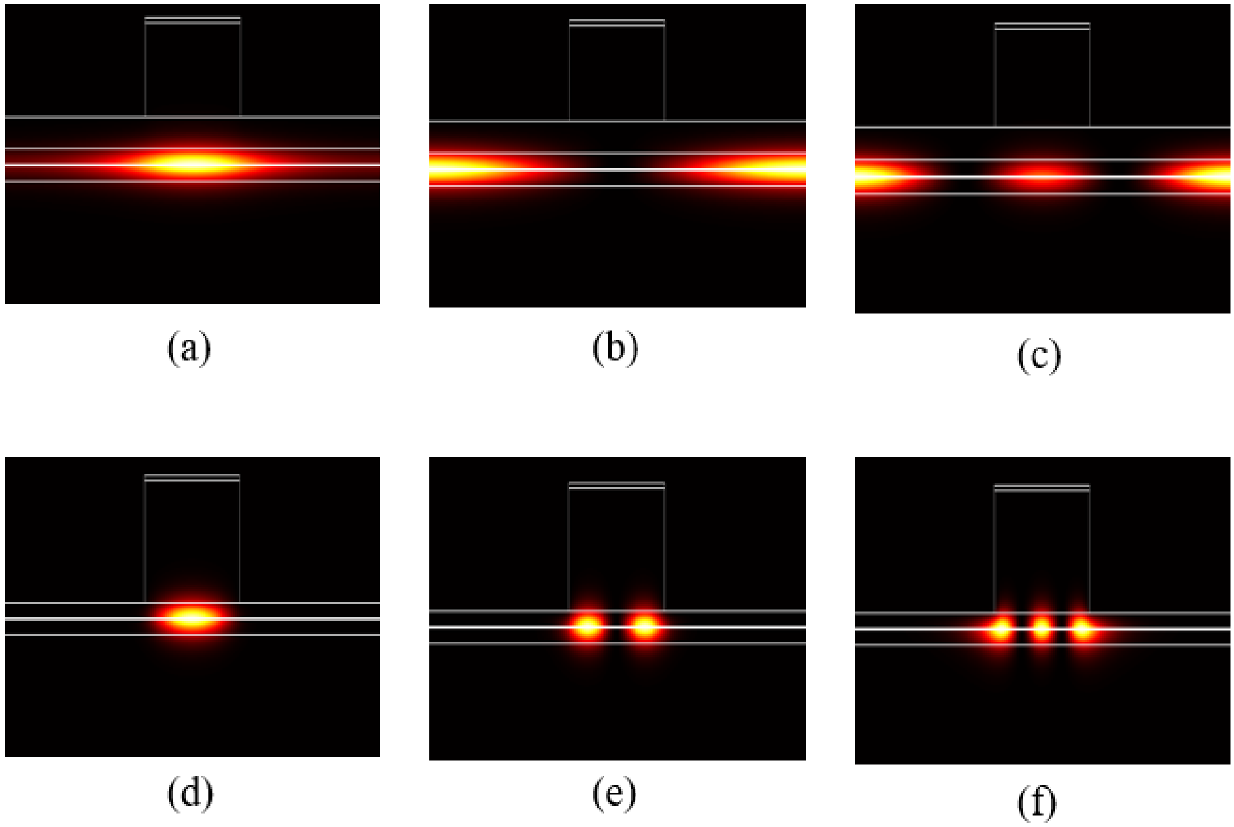

Figure 2.2: Mode profiles [(a) to (c)] for ridge height 1.1 μm and mode profiles [(d) to (f)] for ridge height 1.4 μm for ridge width of 2.5 μm

Due to very close ridge width, the difference in mode confinement due to step refractive index is hard to notice. However, the pattern of increasing mode confinement with increasing ridge depth is observed here also.

The difference in mode confinement with respect to side loss between this two ridge width is shown in the Figure 2.4

As can be seen from the Figure 2.4, with increasing ridge height the side loss of the all the optical modes decreases. This is due to increased step refractive index due to increased ridge height. Therefore, we have to pick the ridge height where the loss of the fundamental mode is zero but also at the same time the loss for the higher order modes is high. This will ensure higher threshold current for higher order modes. (Qiu et al., 2004) For ridge width of

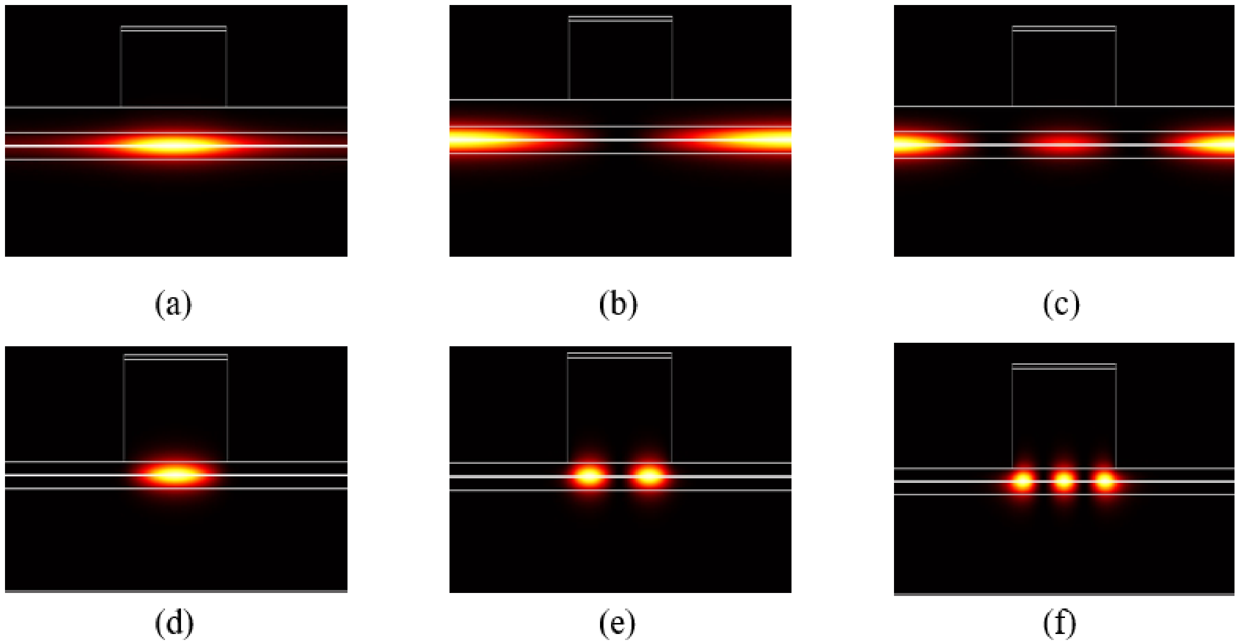

Figure 2.3: Mode profiles [(a) to (c)] for ridge height 1.1 μm and mode profiles [(d) to (f)] for ridge height 1.4 μm for ridge width of 3 μm

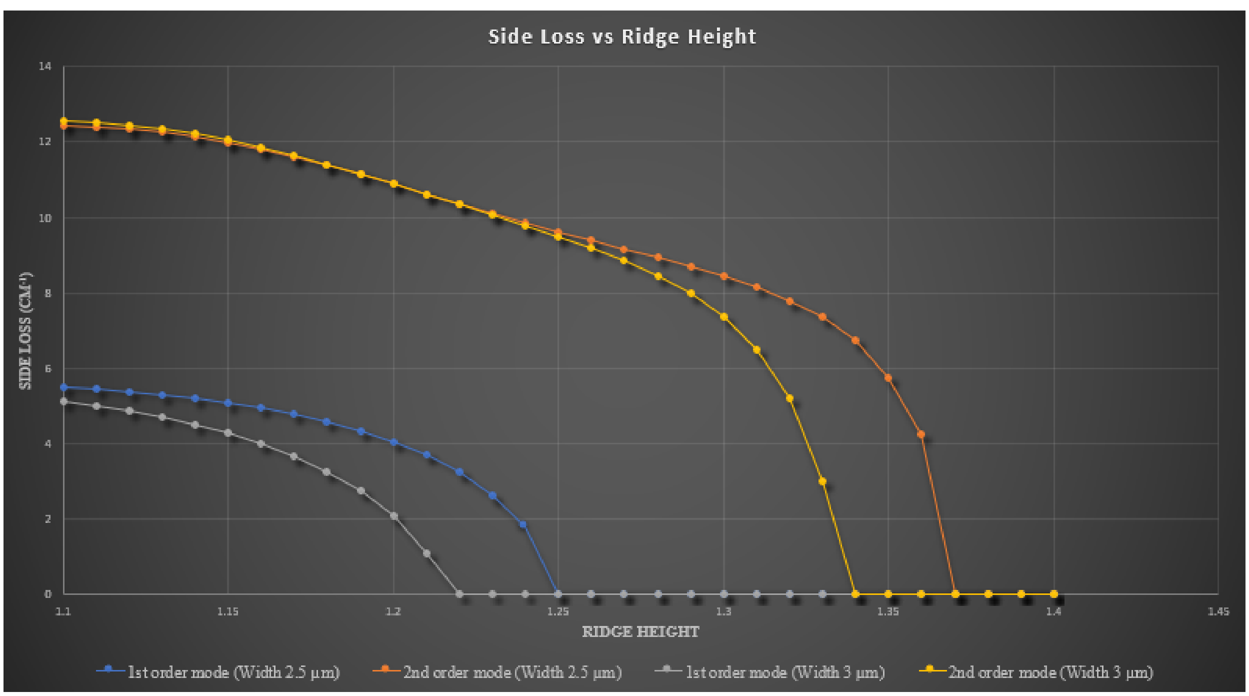

Figure 2.4: Variation of Side loss with increasing ridge depth

3 μm, the ridge height is chosen around 1.2 μm as that gives reasonable loss for both first and second order mode. For the ridge width of 2.5 μm, the depth can be increased as the first order loss for this width goes to zero at 1.25 μm.

CHAPTER 3

FABRICATION

Fabrication of different types of laser i.e., broad area, ridge waveguide and 2-sections are performed in the cleanroom located at the "Natural Science and Engineering Research Laboratories building" or NSERL in The University of Texas at Dallas. Despite few differences during the fabrication process of these lasers, the basic fabrication steps involve preparation of Mask, photolithography for defining features, etching, metallization, thinning and rapid thermal annealing. In the following sections, all these steps will be explained in detail for each of these three different lasers.

3.1 Broad Area Laser

Broad area laser is the simplest device to fabricate and is utilized for characterizing the material quality. The first step is to make the right mask. In the clean room, Heidelberg DWL66 Laser Printer is utilized for making photomasks with resolution 0.6 microns. Photo masks of dimension of 4 to 5 inches are usually patterned. Photomasks for broad area laser involves pattern with repeating rectangular boxes with dimension 75 μm and 225 μm. This pattern of $(75 + 225)$ or 300 μm is repeated for the whole mask. The 75 μm window is used for the metal contact of individual laser whereas the 225 μm is for separating the neighboring lasers. The 75 μm window is clear whereas the 225 μm window is covered with chrome to block the light from passing through it. Figure 3.1 shows the mask for the broad area laser.

The next step involves dicing sample from 3 inch wafer. Diamond scriber is used to dice 10 mm x 10 mm samples from the wafer for maximizing fabrication yield of diode lasers and reducing material loss. The wafers are from IQE and costs around $2650 for a single 3 inch wafer. For cleaving a sample, instead of scribing all along the wafer, a scribe mark is made

Figure 3.1: Broad area laser mask

at the edge. Then, a little force is applied on the wafer and the cleaving follows the 100 orientation of the GaAs plane.

After cleaving the samples need to be cleaned in the cleanroom. The RCA Hoods are used for this. It features temperature controlled cleanup baths, rinse tanks, de-ionized (DI) water and nitrogen spray guns and process timers. Cleaning starts with acetone followed by isopropyl alcohol (IPA) and methanol. Methanol is used in the last place as it dissolves acetone. Finally, DI water is used clean off the chemicals and nitrogen guns are sprayed to dry the samples followed by baking for 40 seconds. If required ultrasonic bath is used for cleaning.

When the standard cleaning process is completed, the samples are ready for the first photo-lithography step. CEE spin coater is used for this purpose. A thin layer of positive photoresist (PR) S1813 is deposited on top of the sample. Speed and acceleration of the spin coater along with the duration of spinning are very important for obtaining uniform photoresist layer. It is found that rpm of 3000 and acceleration of 2000 with a duration of 1 minute of spinning gives the uniform photoresist layer as shown in Figure 3.2. The sample is then baked for 1 minute at 115 °C.

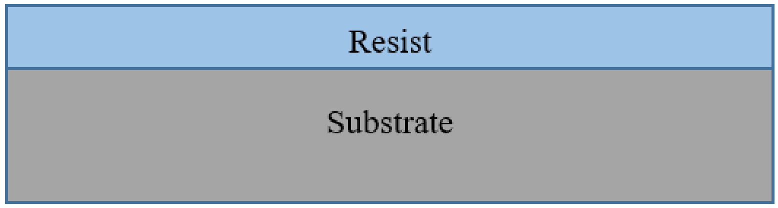

Figure 3.2: Deposition of PR S1813 on substrate

Karl Suss MA6 BA6 contact aligner/printer is used as the lithographic imaging system. A broadband mercury lamp is used for exposing the samples. It has two wavelength options: G line which corresponds to 436 nm and I line which corresponds to 365 nm wavelength. G line is used for positive photoresist PR S1813. After measuring the light intensity of the mercury light, the duration of exposure is determined using the following equation:

$$Time[sec] = \frac{Dose[\frac{mJ}{cm^2}]}{Intensity[\frac{mJ}{sec.cm^2}]} \tag{3.1}$$

In the equation 3.1, the dose represents the required energy for exposing the photoresist and intensity refers to the rate at which energy is being delivered by the mercury light. For S1813, the dose is found around 100 mJ/cm^2 from the manufacturer's data sheet. However, the required perfect dose for a given pattern and the thickness is found by exposing several test samples. Depending on light intensity, which changes over the time, the required time is calculated. The appropriate mask is then placed on the mask holder with chrome side up and the mask holder is put on the wafer chuck and alignment stage. However, as this is the first pattern, there is no requirement of alignment for this step. Once the light is turned on, light exposes the sample through the mask where there is no chrome. This changes the properties of the exposed and the unexposed PR regions. However, this also depends on the type of the photoresist. For positive PR like S1813, the exposed regions become soluble in a solution called developer and the unexposed regions stay. For negative resist like nLOF 2020, the opposite happens.

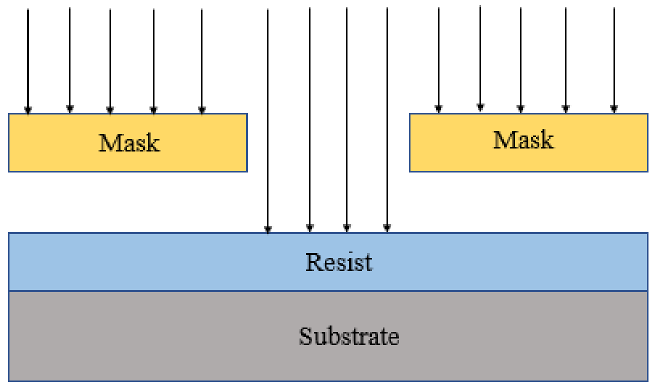

Figure 3.3: Sample under exposure

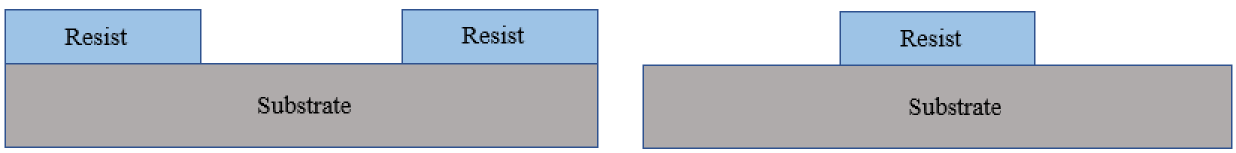

(a) Impact of exposure on positive resist

(b) Impact of exposure on negative resist

Figure 3.4: Samples developed after exposure

The exposed sample is then dipped into a solution called developer, MF-319 for 50 seconds. As can be seen from Figure 3.4a, being positive PR, the exposed region is washed away. The case for a negative resist is shown in Figure 3.4b. The patterns become visible. The sample is then cleaned with DI water and nitrogen gun is used to dry the sample followed by baking for 1 minute.

There are several advantages of baking. Few mentionable ones are

- Evaporates all the solvents of the photo resist (PR).
- Improves adhesion of PR with the surface.
- Smooth out the PR sidewall and improve resolution.

However, over baking should be avoided as that can cause too much reflow of PR causing resolution adversely as shown in Figure 3.5b compared to the normal baking of 3.5a.

Table 3.1: P Contact Metal

Name of Metal	Thickness (nm)
Titanium (Ti)	70
Palladium (Pd)	20
Gold (Au)	200

The Veeco Dektak VIII profilometer is then used to measure the thickness of the developed pattern. A sharp stylus is dragged across the surface of the sample to measure the vertical displacement or thickness.

Next step involves deposition of the metal on the p side of the sample. The Cryo evaporator is used for the thin film metal deposition. The process involves heating of the appropriate metal in a vacuum until it evaporates. The stream of evaporated metal vapor is then deposited on the sample. A sensor is utilized for continuously measuring the thickness of the deposited metal. The Cryo pump is used to pump the chamber down to high vacuum. The recipe for different layers of metal is given in Table 3.1.

The metal is deposited all over the p region as shown in Figure 3.6. The sample is then dipped into acetone. The positive PR dissolves in acetone. Therefore, the metal deposited on top of the PR also goes away as acetone dissolves the PR. Only metal layers deposited on the sample stays. According to the mask, the metal window will be 75 μm. This process is known as lift off. Figure 3.7 shows the sample after lift off.

The thickness of the sample is usually very thick due to the thick GaAs substrate. This thick sample will increase resistance to current injection and also make it difficult to cleave

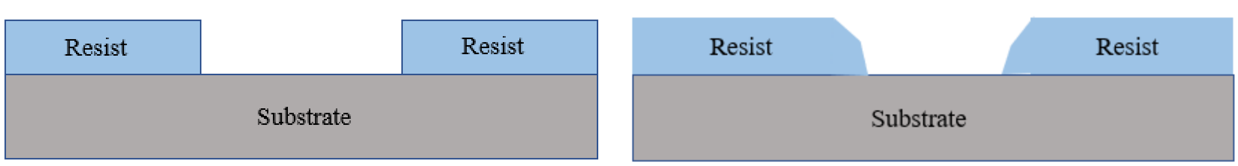

(a) Normal Baking (b) Over Baking

Figure 3.5: Impact of over baking on photoresist

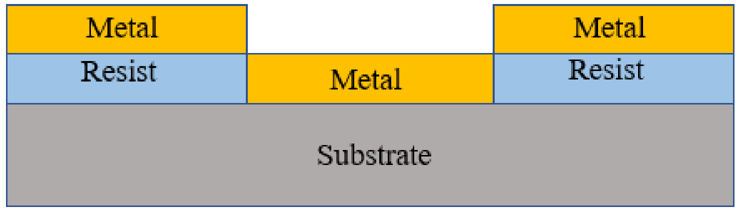

Figure 3.6: Deposition of P contact metal

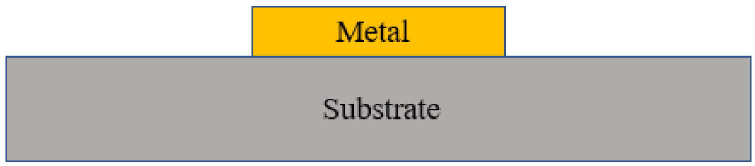

Figure 3.7: Lift off

individual laser bars. To facilitate this, the sample is thinned. Thinning starts by sticking the sample on a glass chuck using glue. The glass chuck is put on the heater and the temperature is set to 190 °C. Once the glass chuck is heated, the sample is placed on the glass chuck by the melted glue. The P side of the sample is the side which will be put on the glass slide or P side down. To make sure that the thinning is uniform, three more small pieces are placed around the glass chuck at 120° angle . The heated chuck is cooled down. On a glass plate, aluminum oxide (Alumina), Al_2O_3 powder is taken with water. The sample is then rotated for thinning. Intermittently the thickness of the sample is measured to reach the thickness of 5-6 mils. At the end of the thinning process, smaller Al_2O_3 powder is taken for finer thinning and also for removing the surface roughness created by the earlier Al_2O_3. Once, the sample reaches the required thickness, the glass chuck is heated again to melt the glue and also to remove the sample from the glass chuck. The P side of the sample is now covered with the wax used in the previous step for thinning. This wax must be removed before going for the N side metallization. The sample is dipped into acetone at 46 °C as long as the wax is not removed. At this stage, the sample should be handled very carefully as the sample is very thin and prone to breaking very easily.

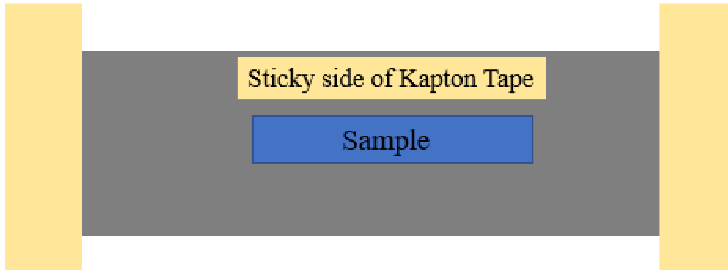

Figure 3.8: Customized Kaptop tape technique used during alignment

It is found that one of the challenges while doing the N side metallization is to pull out the sample out the tape once the metallization is done, the reason being the sample very thin. A technique is used to overcome this problem. A Kapton tape with sticky side up is placed on a glass slide and this tape is placed on the glass slide using two other Kapton tapes at two sides with face down. The technique is shown in Figure 3.8.

The different metal layers for N type metallization is listed in Table 3.2.

Table 3.2: N Contact Metal

Name of Metal	Thickness (nm)
Gold (Au)	14
Germanium (Ge)	14
Gold (Au)	14
Nickel (Ni)	11
Gold (Au)	200

Among different layers of metals, titanium sticks very well to the semiconductor. Palladium (Pd) and platinum (Pt) stops diffusion of gold (Au) in to the semiconductor. And gold (Au) is used for providing very good ohmic contact. The next step is rapid thermal annealing (RTA). The clean room has two MPTC RTP 600 rapid thermal process system which are capable of rapidly heating samples from ambient up to 1200 °C. For our purpose, the samples are heated for 60 seconds at 360 °C with P side down on the Si wafer inside the chamber filled with N_2 gas. This temperature is chosen after extensive measurement of resistance using transmission line measurement technique for finding the minimum resistance.

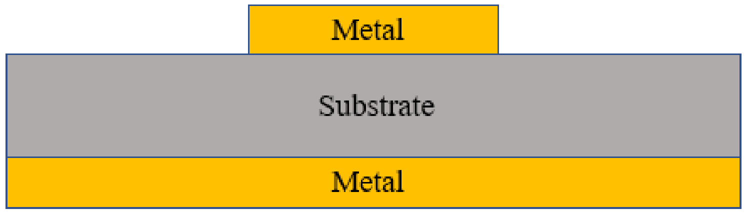

Figure 3.9: Sample after N side metallization

After this step, the samples are ready for cleaving into individual bars of different length for testing.

3.2 Ridge Waveguide Laser

The starting of the ridge waveguide laser is similar to broad area laser(BAL). However, the first mask used for photo lithography is different for the ridge waveguide laser compared to the BAL. Until this step, everything stays same as the BAL.

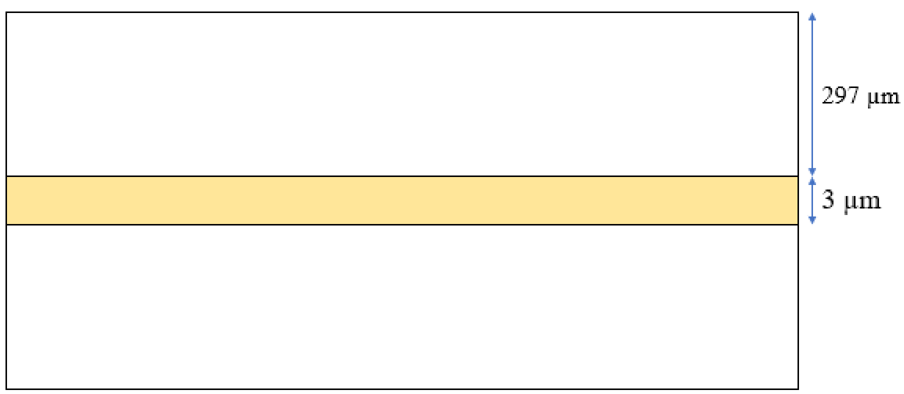

Figure 3.10: Ridge waveguide laser mask

Figure 3.10 shows the first mask for ridge waveguide laser intended for ridge formation. Here, the 3 μm section is covered with chrome so that light cannot pass through it. The remaining 297 μm window is transparent and allows light to pass. The sample after doing this lithographic step is shown in Figure 3.11.

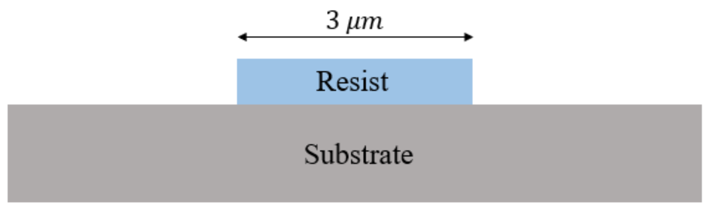

Figure 3.11: Developed sample after using ridge waveguide mask

Now, the ridge is to be formed. Plasma-therm III-V etcher is used for etching the GaAs/AlGaAs material for forming this ridge. Cl_2 and BCl_3 gases are used for etching this sample. Since the 3 μm section is covered with resist, it will not be etched during the etching process. Chlorine is more aggressive than BCl_3. So, flow rate of Cl_2 is kept at 15 sccm and for BCl_3 45 sccm. Electrode temperature is maintained at 25 °C.
The amount of etching depends on the duration of the process. For this sample, our goal is to etch 1.2 μm to make the ridge. Once, the process is completed, the sample is cleaned with acetone to remove the resist. Usually, Acetone removes the resist very easily. However, since this resist is hard baked for 1 minute to withstand the etching, it becomes hard. If acetone is not enough to remove this hard baked resist,chemical EBR-PG can be used. Figure 3.12a and Figure 3.12b show the formed ridge with and without the resist respectively.

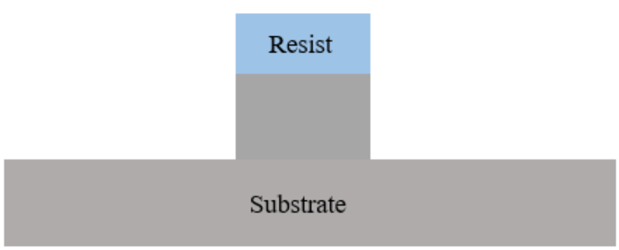

(a) After dry etching

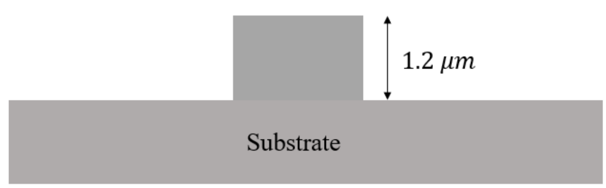

(b) After resist is removed from etched sample

Figure 3.12: Formation of ridge waveguide

The profilometer tool is used for measuring the ridge height but this tool cannot be used to measure the ridge width since the ridge width (3 μm) is smaller than the radius of the stylus (12 μm). The next step is to deposit SiO_2 on the sample. Unaxis 790 PECVD reactor is used for depositing SiO_2 on top of the sample. Around 200 nm of SiO_2 is required to be deposited. After running several test runs, it is found that around 4 minute 30 seconds is required for depositing this amount of SiO_2. Since, SiO_2 is deposited on a custom layered sample, to ease the measurement of thickness of deposited SiO_2, a sample of Si is also put in the chamber. It is this Si sample which is used later to measure the thickness of deposited SiO_2. The Nanospec 6100 thin film thickness measurement system is used which uses spectroscopic reflectometry for measuring the thickness. Figure 3.13 shows the deposited SiO_2 on top of the sample.

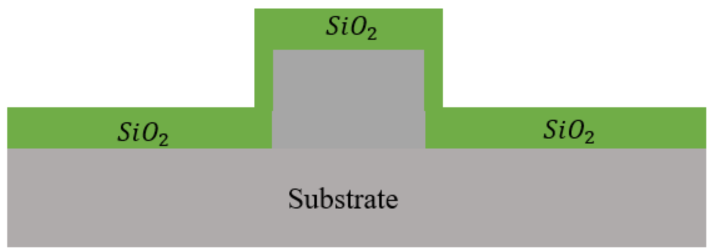

Figure 3.13: Deposition of SiO_2 using PECVD on top of sample

Another photo lithography step is required now to open a window on top of the ridge so that current is only allowed to pass through the ridge. A new mask called contact window mask is used for this purpose as shown in Figure 3.14. This mask is similar to the previous ridge waveguide mask except that the transparent and chromed sections are swapped.

Again, CEE spin coater is used to deposit a thin layer of S1813 resist. The sample is spun at 3000 rpm with acceleration 2000 for this purpose. The sample is then baked for 1 minute. Karl Suss MA6 BA6 contact aligner/printer is used with G line to do the lithography. It can be seen from the CW mask design that the transparent section is now bit smaller than the ridge width. This is done to make sure that the window is definitely within the ridge. This is a very important alignment step. It is also possible to utilize 3.5 μm ridge along with 2.5 μm window to ease the alignment step. The Kapton tape technique described in the broad area laser section is also used here for the alignment process. Since, now 2.5 μm section is transparent, after development, the resist from this section will be gone whereas it will stay in the other sections. The required dose for this step is found to be 93 mJ/cm^2. After the exposure, the sample is developed into MF-319 for 62 seconds. This removes the resist from the top of the ridge within the window of 2.5 μm. However, since the dimensions are very close to the optical limit of the microscope, a little trick is implemented in the design of the mask. The length of the CW mask is made little smaller than the length of the RW mask. Therefore, around the corners it is possible to see whether the contact window is within the ridge or not. Also, there will be markers in the mask which need to be matched for making sure of this alignment. The sample after development will look like as Figure 3.15.

For allowing the current to pass through the window of the ridge, the SiO_2 needs to be etched. Wet etching is used for etching the SiO_2. Buffered oxide etchant (BOE) 7:1 is used in the cleanroom. The resist blocks the wet etchant from etching the underlying SiO_2. Therefore only the SiO_2 in the window is etched. For 200 nm thickness of SiO_2, it is found that around 20 seconds is required to etch. Figure 3.16 shows the structure after wet etching.

The next step will be to remove the resist from the sample. As before, the sample will be dipped into acetone to remove the resist. However, wet etching of SiO_2 might not give a vertical profile like the Figure 3.17. There might be some undercut.

Figure 3.14: Contact window mask for opening window on top of the ridge

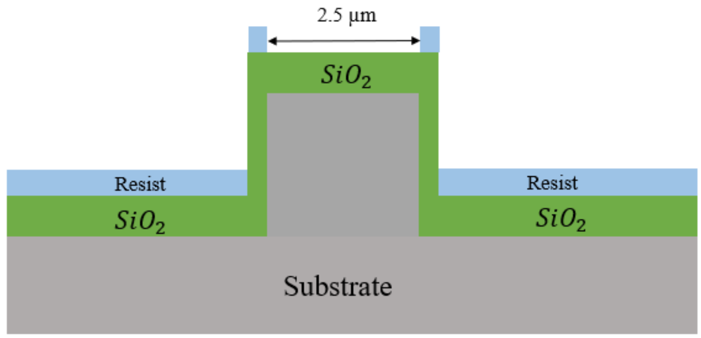

Figure 3.15: After development of sample using CW mask

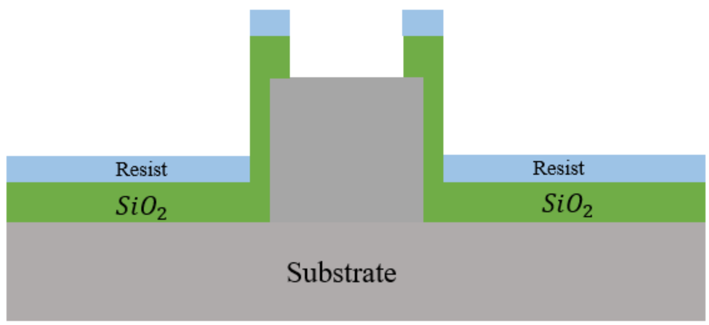

Figure 3.16: Opening of window on top of the ridge using wet etching

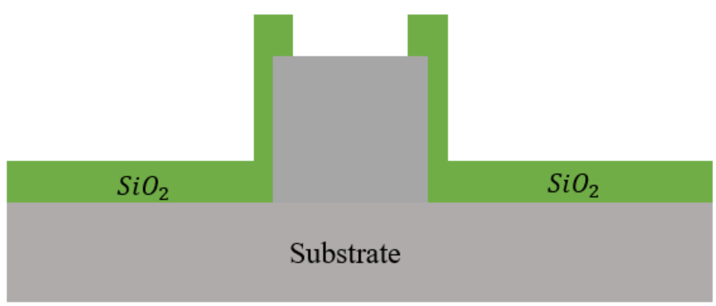

Figure 3.17: Ridge waveguide with open window after removal of resist

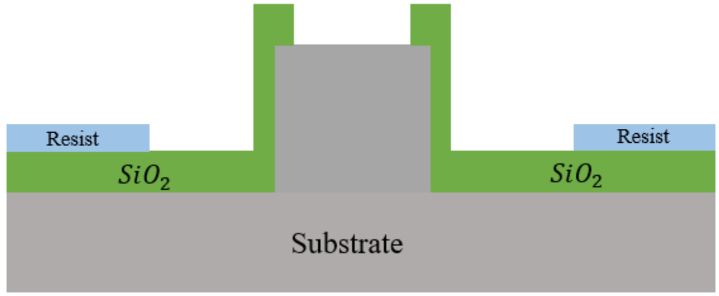

Figure 3.18: After developing using broad area laser mask

The broad area laser mask is now used for doing the P side metallization. The ridge needs to be placed within 75 μm transparent window of the mask. Therefore resist from this region will be removed after the development. Since, 2.5 μm contact window is significantly smaller than the 75 μm window of the broad area laser, alignment is very easy for this step. The sample is covered with thin layer of S1813 again with rpm and acceleration 3000 and 2000 respectively. This time 110 mJ/cm^2 dose is used. The pattern is then developed using MF-319 for 50 seconds. The structure is shown in Figure 3.18.

P side Metallization is the next step to be performed. The same metal layers are used as before. The whole sample will be covered with metal after the metallization as can be seen from Figure 3.19. Lift off will then remove the remove the resist along with metal layers on top of that. For lift off, sample is immersed into acetone. If that doesn't start the liftoff process, ultrasonic bath can be used for a short period of time. After lift-off, the metal will only cover the 75 μm window covering the ridge. Since, most part of the 75 μm window is covered is SiO_2 and the only opening is the 2.5 μm window on top of the ridge, the current will pass through this. The structure is shown in Figure 3.20.

As described in the BAL section, the sample needs to be thinned now. After thinning and cleaning of the sample, N side metallization is done and is shown in Figure 3.21.

Finally, RTA at 360 °C for 60 seconds is performed on the sample. It needs to be remembered that the sample should be put P side down on the Si wafer inside the chamber

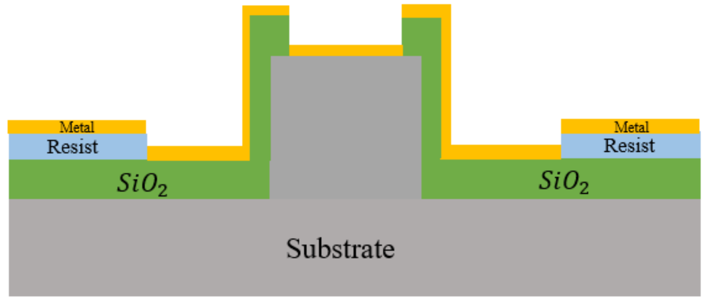

Figure 3.19: P side metallization

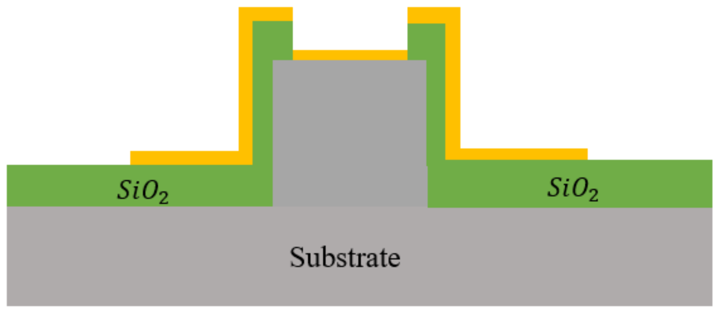

Figure 3.20: Laser structure after lift Off

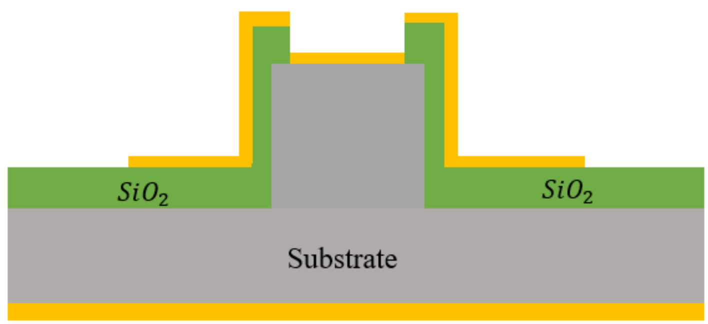

Figure 3.21: Complete ridge waveguide laser structure

filled with N_2 gas. After this step, the sample is ready for cleaving into individual ridge waveguide laser bars.

3.3 2 Section Laser/ Passively Mode Locked Laser

The structure and fabrication of the passively mode locked laser is similar to the ridge waveguide laser except that the contact metal is divided into 2 sections: one section acts as the gain section whereas the other section acts as an absorber. No active component is used for achieving the mode locking here. The gain section is forward biased and the absorber section is reverse biased for this purpose. The gain section is much longer than the absorber section. The fabrication of the 2 section laser is identical to the ridge waveguide laser up to the use of CW mask for opening the window on top of the ridge waveguide laser. For the case of ridge waveguide laser, the BAL mask is used to pattern the P side metal. For the case of passively mode locking laser, an additional lithography step is required. A new Mode Lock (ML) mask is used to create two separate regions with an isolation in between them. The pattern of the new ML mask is shown in Figure 3.22.

Figure 3.22: Passively mode locked laser mask

In this mask, the rectangular boxes are covered with chrome whereas the in between regions are kept transparent. The middle section is later cleaved into two sections thereby making two cleaved laser bars. The separation between the two sections is 10 μm. The sample is then covered with a thin layer of negative resist nLOF 2020. It is spun at a rate of 3000 rpm and 2000 acceleration. The dose for the negative resist is 66 mJ/cm^2. One important thing to remember is that, for the negative resist, the I ($365nm$) line of the lithography tool should be used instead of G ($436nm$) line. The sample is then developed into AZ-300 MIF for 75 seconds. Being negative resist, the exposed regions will stay and the unexposed ones will be removed. So, the resist will stay in between the rectangular boxes. Next, P side metallization is performed using the same metal layers as before. Lift-off is then done which will remove the resist from the region between the boxes along with deposited metal. The top layer of the material is highly doped for improved conductivity. However, for passively mode locked laser, isolation is required between the gain and the absorber section. Though, lift off has removed the metal layers from this region, the highly doped layer will still contribute to the current flow. Therefore, the top layer is required to be removed. From the material database, it is found that the top layer is .25 μm. Another lithographic step along with dry etching is necessary for etching away this top layer.

Again, a thin layer of S1813 is deposited on the sample with rpm and acceleration 3000 and 2000 respectively. Dose is kept at 110 mJ/cm^2. It is developed in MF-319 for 50 seconds. The same ML mask is used this time. However, being positive resist, the resist will be everywhere but in between the regions. As before, the plasma etcher is used to etch the top GaAs layer. Cl_2/BCl_3 chemistry is used as the etchant. Since, only the intermediate regions between the boxes are uncovered, the top layer will only be etched here. One of the issue with using dry etching is that, the etching rate is not stable. Therefore, it is recommended to use a dummy sample for figuring out the sample rate before etching the main sample. The rest of the steps are similar as before for both broad and ridge waveguide laser. The sample is cleaned and thinned. Then N side metallization is implemented followed by RTA annealing. Few pictures of the 2 sections lasers are given in Figures 3.23a and 3.23b. After cleaving, an individual laser bar will look like Figure 3.24:

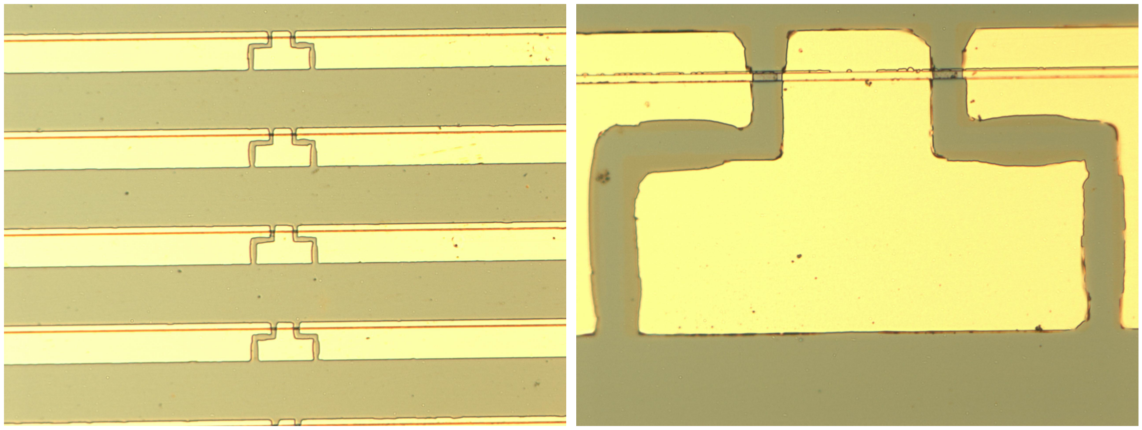

(a) Passively mode locked laser bar (b) Enlarged view of mode locked laser bar

Figure 3.23: Mode locked lasers fabricated in the clean room

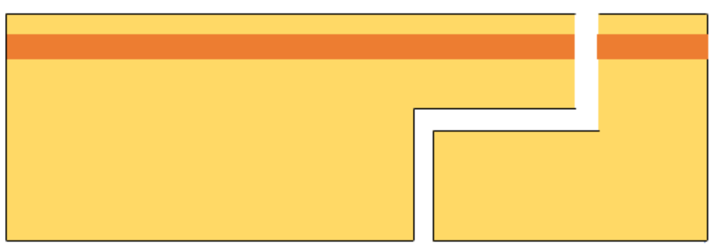

Figure 3.24: Passively mode locked laser bar

CHAPTER 4

CHARACTERIZATION SETUP

Once the fabrication is finished, the next step will be to characterize the semiconductor lasers. In our case, the semiconductor lasers are electrically pumped. Therefore, a complete and integrated setup is required for this electrical pumping and measurement of the optical and electrical characteristics of these lasers. The fundamental setup required is the driving stage for electrical pumping of these lasers. Model 2520 pulsed laser diode test system from Keithley is used for electrical pumping of these diode lasers. The testing system is composed of mainframe and testhead.

The mainframe and the testhead are connected together and they are able to communicate with each other through the computer. There are two interlock circuits: one is remote interlock and the other one is key interlock. Both these interlocks must be enabled for turning on the source output.

Current is applied to the diode lasers through the terminals current output HI and LO. The voltage sense HI and LO terminals are applied across the device under test (DUT) to measure the voltage. There are two detector terminals labeled as detector 1 and detector 2 which will be connected to the photodiode detector. The center conductor or the current input is connected to one photodiode terminal whereas the other photodiode terminal is connected with the inner shield or the BIAS terminal. To avoid the pulse degradation while driving the laser diodes, following things should be remembered (Keithly, 2002):

- 15 Ω coaxial cables should be used
- The total length of both cables should be well within the recommended length of 40 cm.
- At the DUT, the shields of the four cables should be connected together.

- For avoiding magnetic coupling, the voltage sense cables should be placed from the current output cables as far as possible. Twisting of the sense cables will reduce the electro-magnetic coupling further.

- Length of the unshielded signal lines should be minimized.

- voltage sense leads should be placed very close to the body of the DUT.

This system along with a photodetector is all required for the light, current and voltage (LIV) characterization. The laser diodes are placed on the stages. Now, the current and voltage terminals from the testhead are connected with the probes. The probes are then used to contact the laser diodes. The diode is placed n side down on a gold plated surface. The LO terminals of both current and voltage are placed on this surface thereby providing negative connection to the diodes. The positive terminal of the voltage sense is shorted with the positive terminal of current. The positive terminal of the output terminal is then placed on the p side of the diode laser. Micro blocks from Thorlabs are used to hold the stages. Another micro block holding a photo detector is placed in front of the laser diode. The detector will be connected with any one of the detector terminals of the testhead. A LabVIEW interface is used for controlling this testing system. DC or pulsed current can be used for testing the diode lasers. Also, it can varied between sweep and fixed mode. The different combinations are shown in Figure 4.1:

Before the integration of the cooling system, it is recommended to drive the laser in pulsed mode to avoid the detrimental effect of heating. When the pulses are triggered and current is driven for a certain range, the light power can be measured by the photodetector and also the voltage across the DUT can be measured. The power can also be measured using the power meter PM100D from Thorlabs. This meter is connected with an integrating sphere photodiode power sensors which are insensitive to beam shape, divergence and entrance angle.

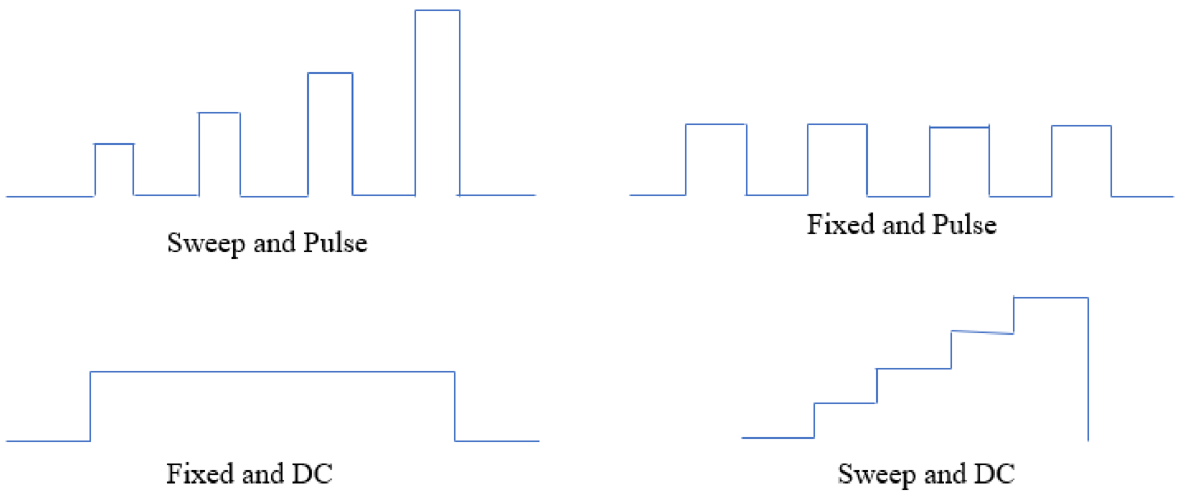

Figure 4.1: Different driving current modes

This power meter will measure the average power. Depending on the duty cycle we can measure peak power from the average power.

$$PeakPower = \frac{Energy, E}{Duration, \Delta t} \tag{4.1}$$

$$AveragePower = \frac{Energy, E}{TimePeriod, T} = E * f \tag{4.2}$$

Solving for Energy E gives,

$$PeakPower * \Delta t = AveragePower * T \tag{4.3}$$

$$Dutycycle = \frac{\Delta t}{T} = \frac{AveragePower}{PeakPower} \tag{4.4}$$

$$PeakPower = \frac{AveragePower}{DutyCycle} \tag{4.5}$$

The next important step is to integrate the thermal cooling so that we can drive the diode lasers in DC mode. The LDC-3724C precision laser diode controller is used for controlling the temperature using TEC cooling. A thermoelectric Peltier cooler is placed on the micro block. Depending on the current flow, one side of the Peltier cooler will be heated and the other side will be cooled. A metallic stage is placed on the Peltier cooler. It should be made sure that this is the side that is cooled. The sample is placed on this stage. A sensor is placed very close to the sample to monitor the temperature which is then used to feedback into the laser diode controller. Using this feedback, the precision laser diode controller is able to maintain a stable temperature. The setup is now ready for measurement of power in both pulse and DC mode. One of the issues with measuring power using the power meter is that, we need to define the wavelength of the light there. Therefore, in order to use the power meter we need to measure the wavelength first. An optical spectrum analyzer (OSA) is used for this purpose. MS9740A-009 optical spectrum analyzer from Anritsu is the one we have in our lab. It supports both single mode and multi mode fiber. Light needs to be coupled from the diode laser into a single mode or a multi-mode fiber which will be input to the OSA. The wavelength range is from 600 nm to 1750 nm with several resolution options e.g. .07, .1, .2, .5 and 1 nm.

One of the most important steps in the characterization setup is to setup the coupling of light into multi-mode and single mode fiber. Coupling into multi-mode fiber is lot easier compared to single mode fiber. Aspheric lenses are utilized for coupling light into the fibers. Selection of aspheric lens is very crucial. In the first place, it is desired to collect as much light as possible by the lens. Since, the light emitted by diode laser diverges rapidly, it is a good idea to start with a very high numerical aperture lens. Numerical aperture is defined as in 4.6

$$NA = n * sin\theta \tag{4.6}$$

Where, n is the refractive index of the material of the lens and θ is the half angle of the cone of the light that can enter or exit the lens as in Figure 4.2. When selecting the

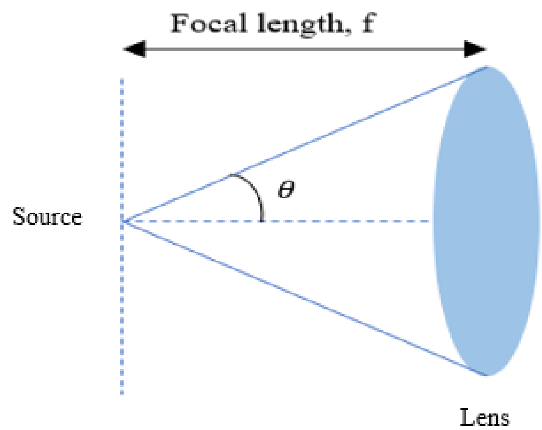

Figure 4.2: Numerical aperture of an aspheric lens

collimating aspheric lens, the NA of the lens should be higher than NA of the diode laser. However, the divergence angle for the diode laser is different in the horizontal and the vertical direction. The vertical divergence is significantly higher than the vertical one. So, this is the angle that should be considered for numerical aperture calculation.

The first aspheric lens will collimate the diverging light into a collimated beam. The next aspheric lens has to focus this collimated beam into the core of the fiber. It is required that the focused beam should match the mode field diameter of the fiber. The required focal length of the lens can be calculated using the equations 4.7 4.8 (Thorlabs, 2018) . Also, a suitable anti-reflective coating should be selected.

$$MFD = \phi_(spot) = \frac{4 * \lambda * f}{\pi * D} \tag{4.7}$$

$$or, f = \frac{\pi * D * MFD}{4 * \lambda} \tag{4.8}$$

Where, f = focal length of the lens, D = Collimated beam diameter, λ=wavelength and MFD = Mode Field Diameter

The complete setup is shown in Figure 4.3

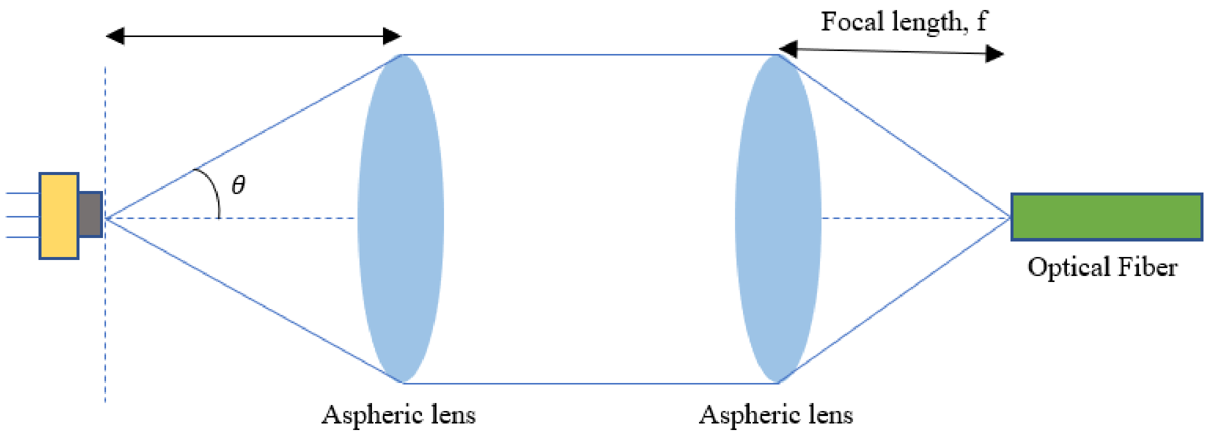

Figure 4.3: System for coupling light in to the fiber

For our case, the collimating aspheric lens was selected with NA .6 and the focusing aspheric lens was selected with NA .16. The coupled light into the optical fiber is then input into the OSA. This measures the wavelength of the input light.

The autocorrelator is used to measure the short optical pulses emitted from the passively mode locked diode lasers. FR-103 XL is a dispersion free autocorrelator which can measure the temporal width of the pulses. By utilizing the highly reflective metallic-coated optics, a very high resolution of < 5 femto second is obtained. It is only limited by the thickness of the non linear crystal. For using the autocorrelator, it is necessary to couple light in to a single mode fiber. The light is then split by a pellicle beam splitter after coming from the single mode fiber output. One of the rays is directed to a rotating mirror assembly which linearly delays the time in one of the arms. The other beam travels towards a mirror. After being reflected from this mirror, the beam travels towards a reflector. Finally this retro-reflected beam hits again in the beam splitter. The two beams now being reflected from an angled mirror, hit the nonlinear crystal. There is an opening after this nonlinear crystal which is covered with an appropriate filter. The second harmonic light generated from the interactions of the two beams in the nonlinear crystal enters through this opening. The amplitude of the

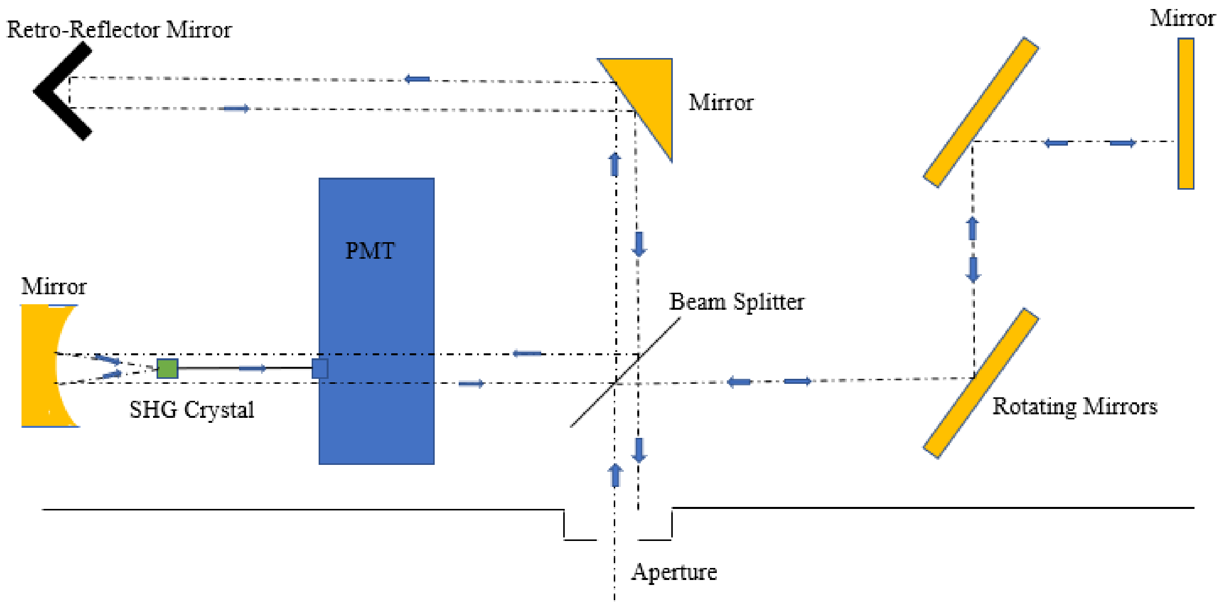

Figure 4.4: Autocorrelator internal housing

signal can be amplified by increasing the gain of the PMT housing. The complete setup for the autocorrelator is shown in Figure 4.4:

Now, for achieving mode locking a reverse bias is required to be applied to the absorber section of the diode laser. For this, a voltage supply is utilized. The current from the testhead is applied to the gain section and reverse bias from the voltage supply is applied to the other section by connecting the source to a pair of probes. This completes the characterization setup for the diode lasers.

CHAPTER 5

RESULTS

Characterization of the diode laser starts with the LIV test. The setup for the LIV testing is described in the previous section. The laser diodes are cleaved into different lengths. LIV testing is started with the broad area laser. The cleaved length is 1 mm. The sample is put on the metal plate which TEC cooled stage. Driving current is applied from the mainframe 2520 system and also the voltage across the device is measured at the same time.
In this section, the characteristic of the diode lasers will be based on threshold current, output power, temperature, emission wavelength and cleaving length of the diode laser. Broad area laser is the simplest to fabricate. It is usually employed to determine the quality of a semiconductor material by measuring threshold current density. It doesn't have any structure for confining current. There are several factors that can affect the threshold current density of this laser (Agrawal and Dutta, 2013). Doping of the active region with P type dopants is one of these. Increased P doping will significantly increase the threshold current due to non-radiative Auger recombination and also due to increase in optical absorption (Agrawal and Dutta, 2013). For this reason, it can be seen from the material database that the active region and also the surrounding barrier layers are not doped. A typical light-current characteristic of a broad area laser is shown in Figure 5.1

The red line indicates the measured voltage across the diode laser. For the linear portion of the red curve, dividing the laser voltage with the driving current will give the series resistance. The green curve shows the output light characteristics. The threshold current is around 160 mA. The output power increases linearly up to around 290 mA after which there is a kink in the light output characteristics. This change can occur due to one or more of the followings (Agrawal and Dutta, 2013) (Achtenhagen et al., 2006):

- Transition from fundamental to higher order modes

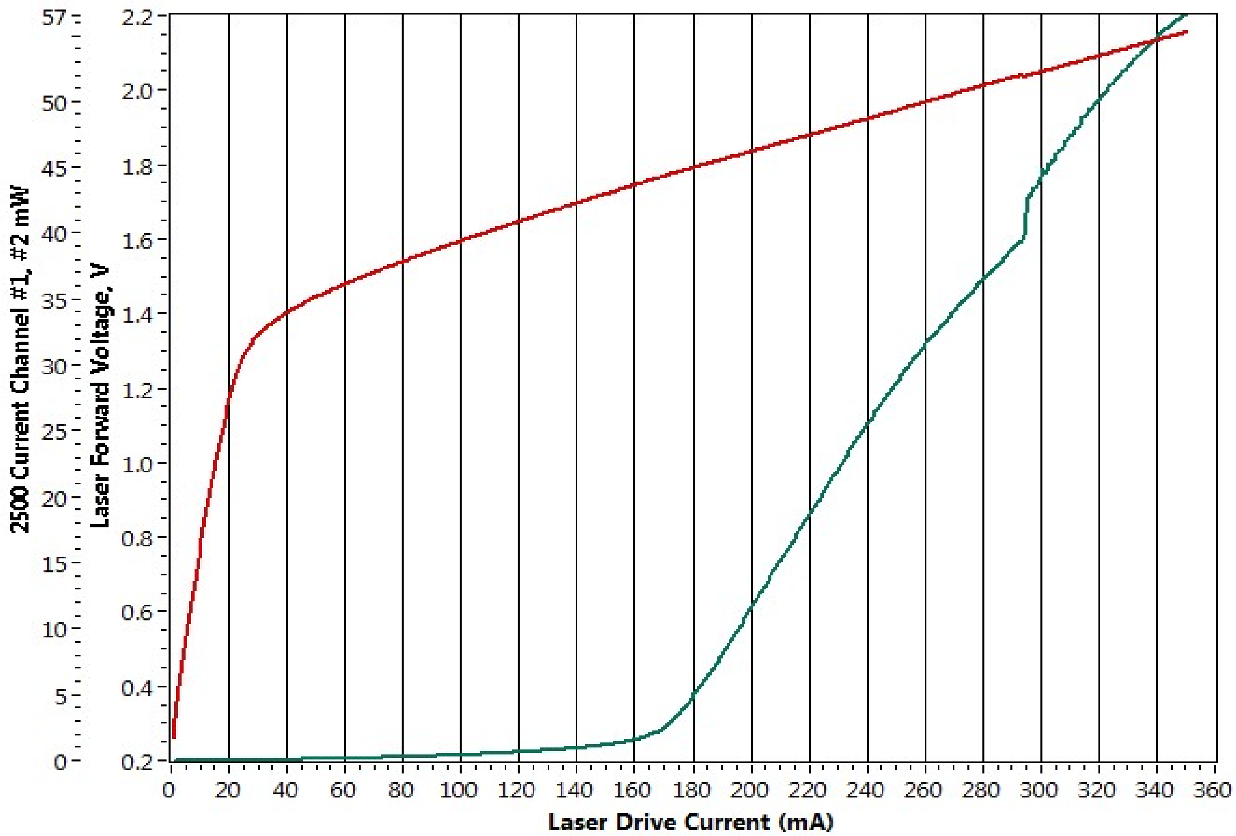

Figure 5.1: LIV characterization of broad area laser

- Transition from the TE to TM mode
- Optical mode moving along the junction plane

This is not a desirable property of the diode laser. This impacts severely the coupling of light from the diode laser in to an optical fiber.The other thing about this light output is that, below the threshold, the increase in output power is very low. In this region the laser is working as Light Emitting Diode (LED) and spontaneous emission is mostly taking process here.

The slope of LI curve conveys one very important information about the diode laser. It is desirable to get as much light output as possible for a given current input. The higher the slope of the LI curve after the threshold, the more efficient the laser diode is. The slope of the LI curve is given by,

$$\text{Slope of LI curve} = \frac{\Delta P}{\Delta I}\frac{mW}{mA} \tag{5.1}$$

Therefore, from Figure 5.1

$$slope = \frac{20-0}{225-160} = \frac{20}{65} = .31\frac{mW}{mA}$$

Since, there are two facets of a diode laser, therefore

$$slope = 2 * .31 = .62\frac{mW}{mA}$$

From this parameter, a very important parameter can be derived known as external differential quantum efficiency (EDQE), η_d. It indicates the efficiency of a diode laser for converting the injected electron hole pairs into useful light or photons emitted from the device. A perfect diode laser should convert every electron hole recombination into useful light. However, this perfect device doesn't exist. This parameter is a ratio between a real device and a hypothetical perfect device. If the emitted wavelength is λ, for a single photon the emitted energy will be $E = \frac{hc}{\lambda}$. Now, if charge of q coulombs flow in one second and generate E energy per second, the slope for perfect laser diode will be

$$slope = \frac{\frac{hc}{\lambda}}{q}$$

The ratio between this two ratios will give the external differential quantum efficiency (EDQE). Therefore,

$$\eta_d = \frac{\frac{\Delta P}{\Delta I}}{\frac{hc}{q\lambda}} \tag{5.2}$$

Therefore, for the previous mentioned diode laser with wavelength 893 nm, the external quantum differential efficiency will be

$$\eta_d = \frac{.62}{\frac{1.24}{.893}} = .4465$$

$$\eta_d = 44.65\%$$

The threshold current depends on the length of the laser. The threshold current density is obtained by dividing the threshold current of a diode laser by the area of the diode laser. The lower the threshold current density the better the diode laser is. The width the fabricated broad area lasers is 75 μm. Now if the length is 1 mm, threshold current of 160 mA will give

$$\text{Threshold current density, } J_{th} = \frac{160mA}{75\mu m * 1mm} = 213.33\frac{A}{cm^2}$$

The external quantum differential efficiency also depends on the dimensions of the diode laser. Therefore in order to compare laser devices it is necessary to define parameters that are independent of dimensions. Internal quantum efficiency and internal loss are such two important parameters.

The internal quantum efficiency (IQE) is defined as the efficiency of a diode laser for converting the electron-hole pairs into photons or light within the device. The difference between IQE and EDQE is that, the IQE doesn't depend on the dimensions of the diode laser. Therefore, if IQE is 80% it means that among 100 electron-hole recombination only 80 are converted into light and the remaining 20 are converted into some other form, mostly heat. However, these 80 photons might not make it out of the device as they can be reabsorbed due to several internal losses before leaving the facets of the diode laser. Due to this, the EDQE will always will be less than IQE. It is defined by the symbol η_i. Now, if the internal loss is α_i, the relation between the EDQE and IQE will be given by (Mobarhan, 2018),

$$\frac{1}{\eta_d} = \frac{1}{\eta_i}[1 + \frac{\alpha_i}{ln\frac{1}{R}}L] \tag{5.3}$$

The Table 5.1 shows the measured inverse of the EDQE for different length of diode lasers. The plotting is shown in Figure 5.2. As can be seen from the equation 5.3, extrapolating

Table 5.1: Table for finding Internal Loss, α_i and IQE

Cavity Length(μm)	Slope Efficiency(2 mirrors) $\frac{mW}{mA}$	EDQE (η_d)	Inverse of EDQE $\frac{1}{\eta_d}$
650	.85	0.612137097	1.633620974
800	.84	0.604935484	1.653068842
900	.8	0.576129032	1.735722284
1000	.78	0.561725806	1.780227984
1230	.7	0.504112903	1.983682611

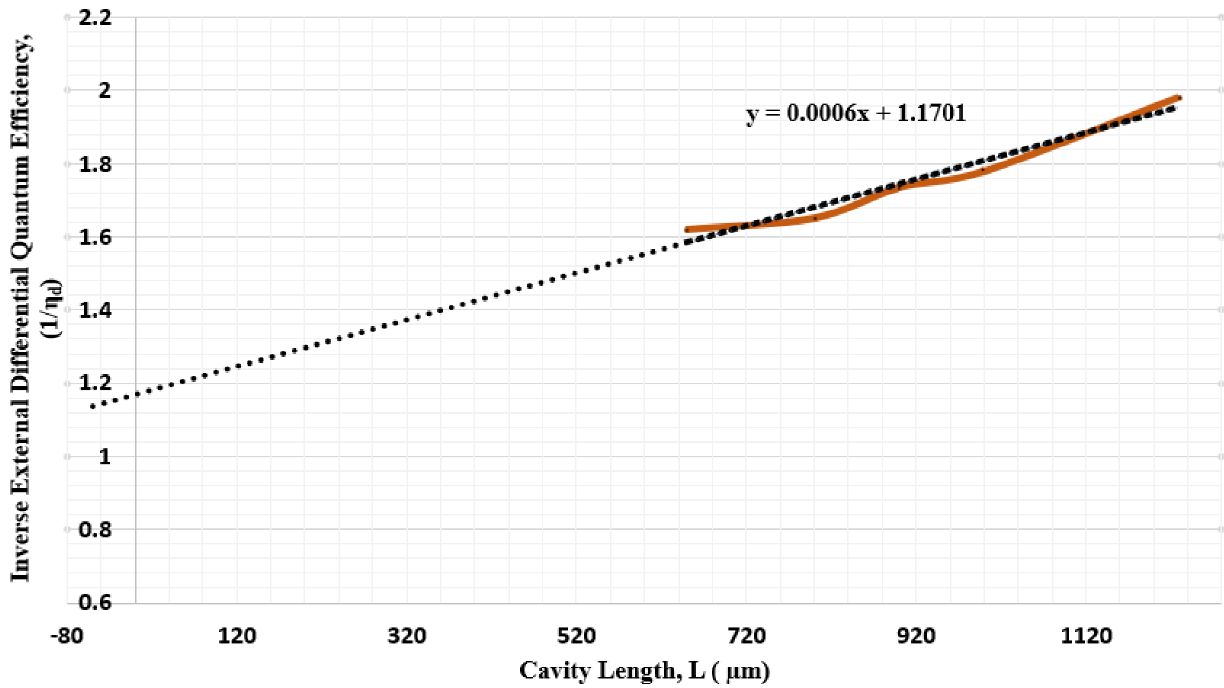

Figure 5.2: Dependence of inverse external differential quantum efficiency on cavity length

to the length 0, EDQE will be equal to IQE. Also, if we multiply the slope of the straight line with $ln(1/R)\eta_i$, that will give us the internal loss, α_i. The backward projection of the straight line hits the Y axis at value 1.1701. Taking the inverse of this value, gives us,

$$\text{IQE} = \frac{1}{1.1701} = .855$$

$$\text{or, IQE} = 85.5\%$$

The slope of the line is .0006. As described above,

$$\alpha_i = \frac{.0006 * .855 * ln\frac{1}{.32}}{10^{-4}} = 5.85cm^{-1}$$

As these two parameters are independent of laser dimensions, lasers made out of different material can be compared based on these parameters.

Since, threshold current density depends on the length of the cavity, the comparison between two different set of diode lasers will be imperfect based on threshold current density. To overcome this problem, threshold current density for different length of diodes are measured. These values are then plotted against the inverse of the cavity length. The extrapolated line hits the y axis at a certain value. This represents the hypothetical value of the threshold current density when the cavity is of infinite length. This parameter can be used for comparing the threshold current density of devices made from different materials. Table 5.2 shows the data of threshold current density for different length of diode lasers.

Table 5.2: Table for finding Transparency Threshold Current Density J_o

Cavity Length(μm)	Inverse of Cavity Length	Device Area (cm^2)	Threshold Current(A)	Threshold Current Density (A/cm^2)
0.065	15.38461538	0.0004875	0.104	213.3333333
0.08	12.5	0.0006	0.118	196.6666667
0.09	11.11111111	0.000675	0.13	192.5925926
0.1	10	0.00075	0.14	186.6666667
0.123	8.130081301	0.0009225	0.165	178.8617886

As can be seen from the Figure 5.3, the fit line intercepts the y axis at value 139.91. Therefore, the threshold current density for infinite length is 139.91 A/cm^2.

Till now, all these measurements of diode lasers were carried out at room temperature. However, it is very important to analyze the diode lasers performance at elevated temperature. Particularly for high power lasers, it is very important to keep track of lasers degradation with rise in temperature. For this reason, here the performance of the fabricated lasers are measured at different temperatures. Figure 5.4 shows the LI curves of diodes lasers for different elevated temperatures.

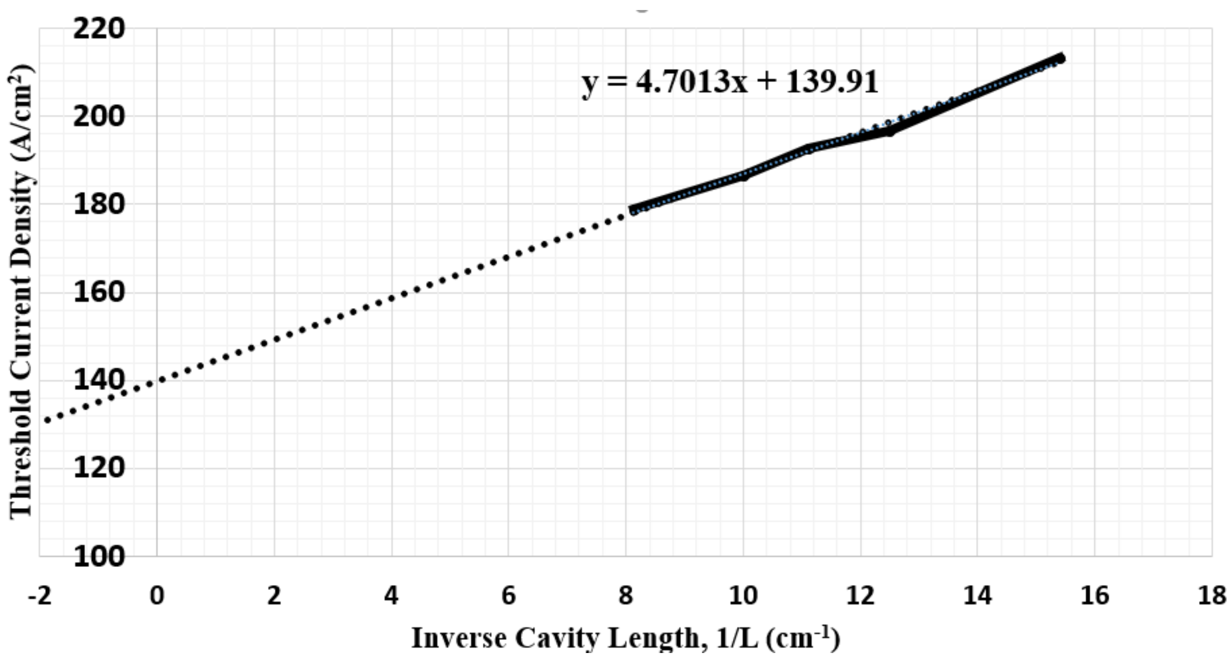

Figure 5.3: Dependence of threshold current density, J_{th} on the inverse of the cavity length

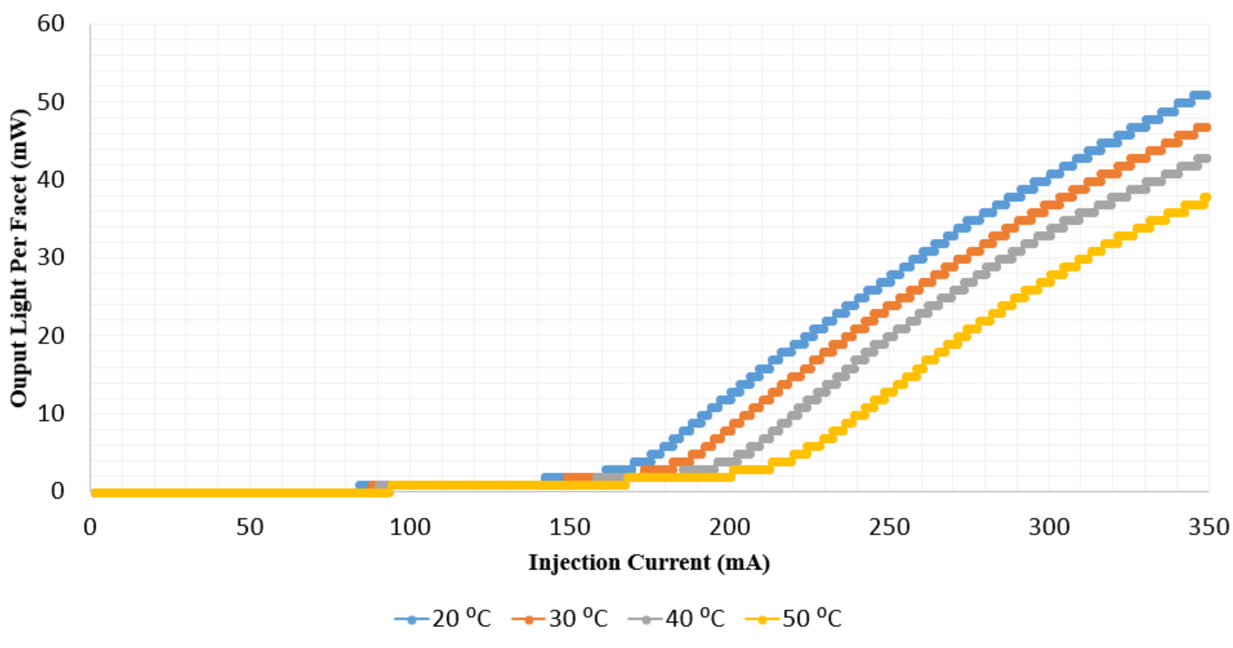

Figure 5.4: Output light characteristic of diode laser for various operating temperatures

As can be seen from the Figure 5.4, with increasing temperature the threshold current of the same device increases with decreasing slope efficiency. A parameter called characteristic temperature, T_o is used to measure the sensitivity of the diode laser. The higher value of T_o indicates that the threshold current density and the EDQE of the diode laser will not increase rapidly with increasing temperature. This in turn means that the devices will be more thermally stable. To measure this parameter, the threshold current density is measured for different temperatures and then plotted. Table 5.3 shows the data of threshold current densities for different temperatures:

Table 5.3: Threshold Current Density for different operating Temperatures

Temperature(^0C)	Threshold Current (I_{th})	Threshold Current Density (J_{th})	Ln (J_{th})
10	0.16	213.3333333	5.362855888
20	.167	222.6666667	5.405675885
30	.175	233.3333333	5.452468046
40	.185	246.6666667	5.508037898
50	.194	258.6666667	5.555540232
60	.203	270.6666667	5.600888051

The corresponding plot of logarithm of threshold current density vs temperature is shown in Figure 5.5:

Now, the relation between the threshold current density, J_{th} and the characteristic temperature, T_o is given by the following equation (Mobarhan, 2018):

$$J_{th} = J_0 exp\frac{T}{T_0} \tag{5.4}$$

In the equation J_0 and T_0 are two constants. Solving for T_0 gives us (Mobarhan, 2018),

$$T_0 = \frac{\Delta T}{\Delta ln J_{th}} \tag{5.5}$$

The slope of the fit line is .0048. Taking the inverse of the slope gives,

$$\text{Characteristic Temperature, } T_0 = \frac{1}{.0048} = 208.3^0C \tag{5.6}$$

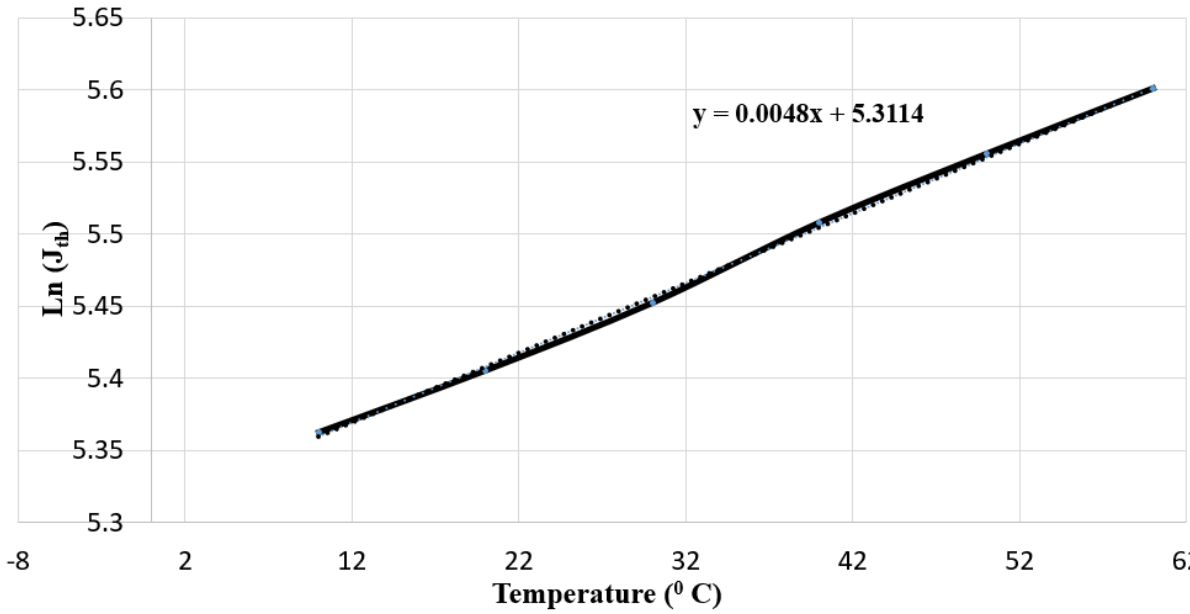

Figure 5.5: Logarithm of threshold current density vs temperature for finding characteristic temperature

There is also a linear relation between the peak wavelength of a laser diode and the temperature. As the temperature is increased linearly, the peak wavelength shifts to higher value. This shifts is also measured for the fabricated BAL lasers. Table 5.4 shows the tabulated data and the Figure 5.6 shows the pattern for this:

Table 5.4: Shift of Peak Wavelength with Temperature

Temperature(^0C)	Wavelength (nm)
20	897.22
25	898.8
30	900.56
35	902.36
40	903.8
45	905.16

Finally, the optical spectrum of the emitted light from the BAL is measured using the optical spectrum analyzer. It is shown in Figure 5.7:

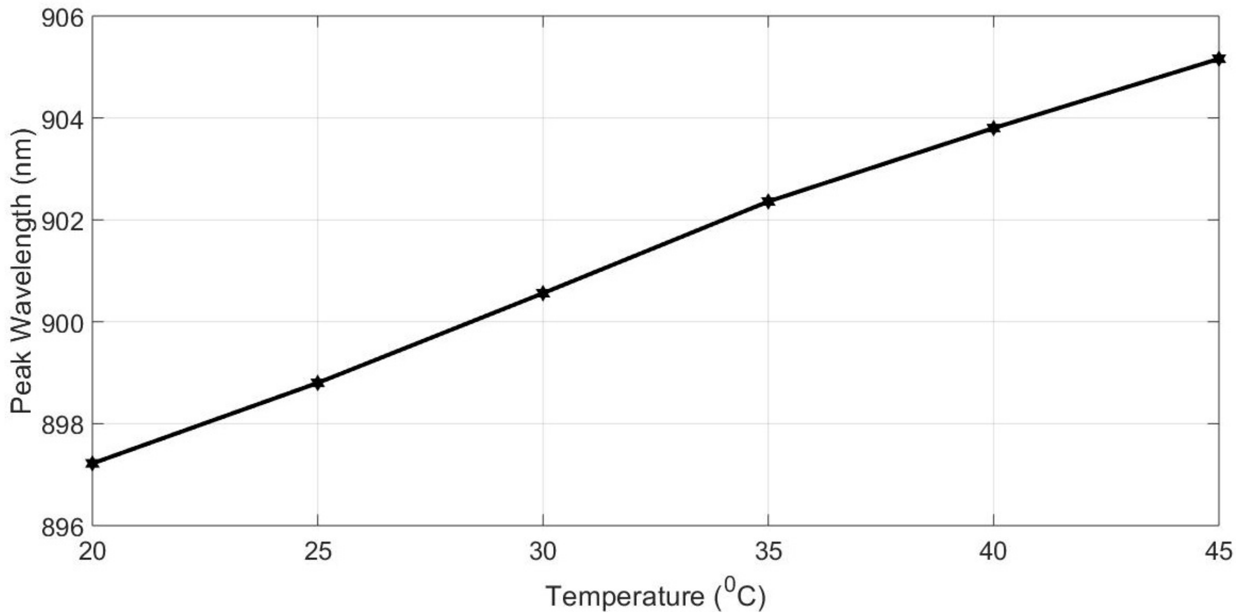

Figure 5.6: Shift of peak wavelength with increasing temperature

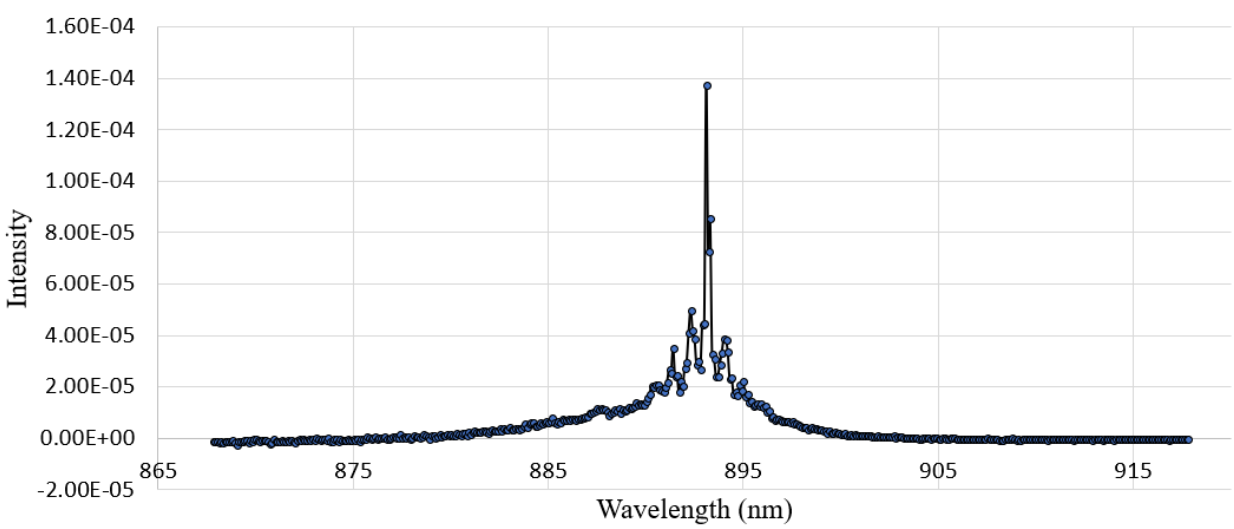

Figure 5.7: Optical spectrum of broad area laser

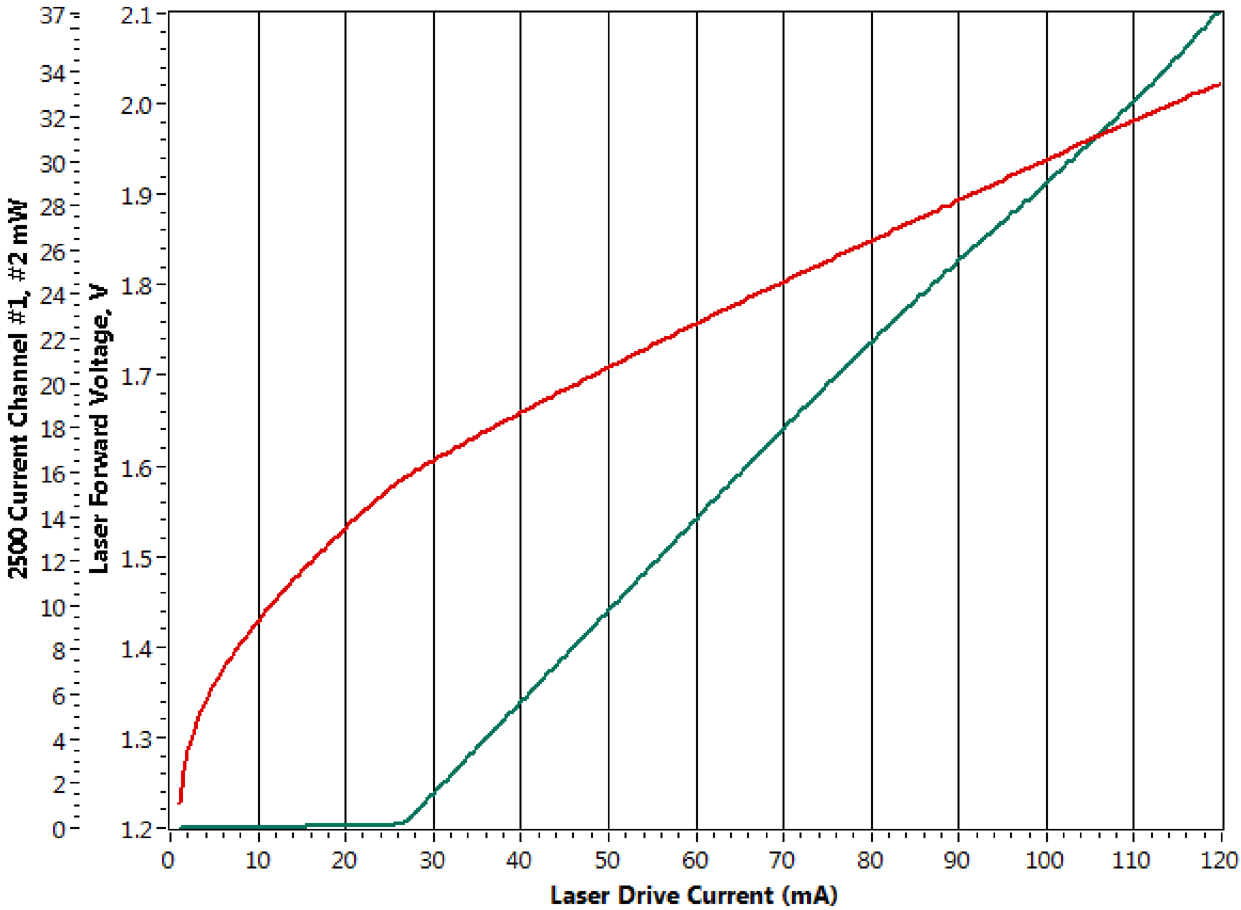

Figure 5.8: LIV characterization of ridge waveguide laser

From the figure it can be seen that the peak wavelength is 892.8 nm.

Now, the LIV characterization is measured for the ridge waveguide laser. The width of the laser is 3 μm and cleaved length is 1 mm. It is shown in Figure 5.8

The first thing to notice from the Figure 5.8 is that for the same 1 mm cavity length the threshold current has decreased significantly to 26 mA compared to 160 mA of broad area laser. This is due to confinement of carriers into a small ridge opposed to BAL. For ridge waveguide lasers, Slope of LI curve:

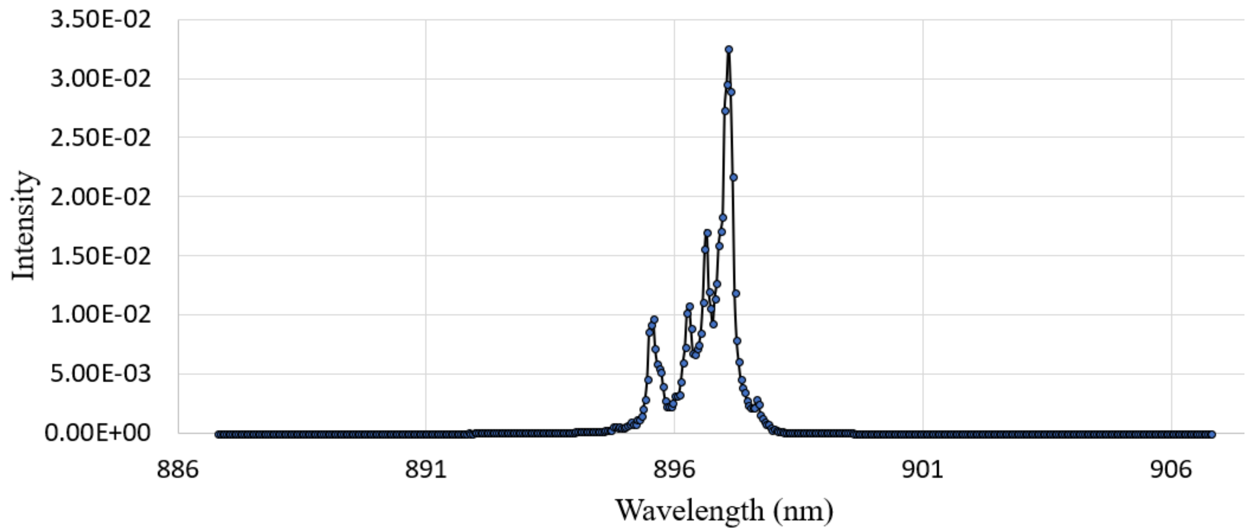

Figure 5.9: Optical spectrum of ridge waveguide laser

$$\text{slope} = \frac{\Delta P}{\Delta I} = \frac{10-0}{50-26} = .42\frac{mW}{mA}$$

For two mirrors,

$$Slope = 2 * .42 = .84\frac{mW}{mA}$$

As ridge waveguide lasers emit high output at very low driving current, heating is not a very big concern for this kind of laser. However, all the measurements are done at room temperature. The optical spectrum of the ridge waveguide laser is shown in Figure 5.9

The measured peak wavelength is 896.8 nm.

Finally, LIV characterization and optical spectrum measurement of 2 section lasers are made. The LIV measurement is done by forward biasing the gain section and reverse biasing the absorber section. For Figure 5.10 the absorber section bias is not applied.

The length is also 1 mm and width 3 μm. However, within the length there is an absorber section of 30 μm and an isolation of 10 μm between the gain and the absorber section. As can be seen, the threshold current density is higher for the 2 section laser compared to ridge

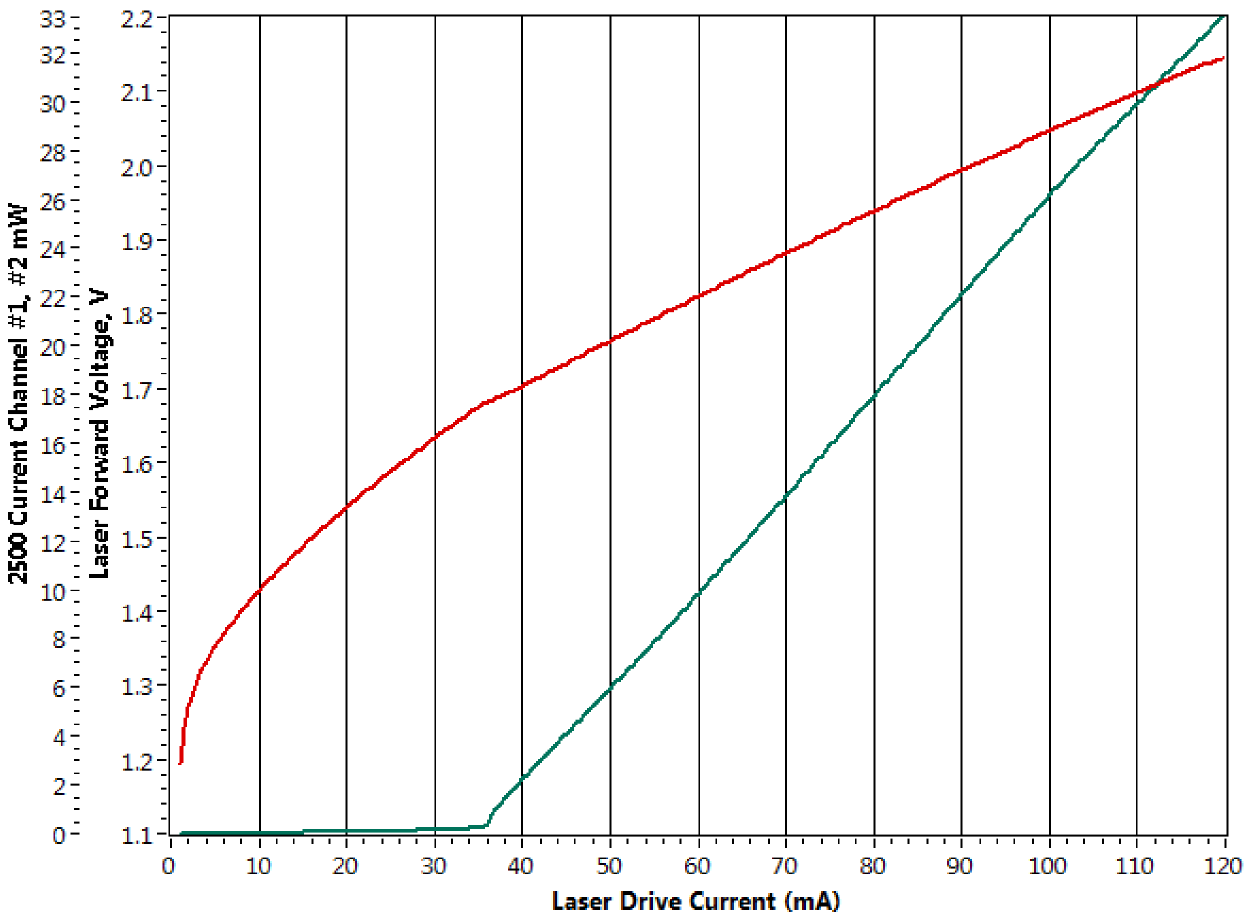

Figure 5.10: LIV characterization of 2 section laser

waveguide laser due to this absorber section. The threshold current is 36 mA and slope efficiency is .8 mW/mA. The optical spectrum of the 2-section laser is shown in Figure 5.11 with peak wavelength 898.46 nm.

The previous Figure 5.10 shows the output characteristic curve without the application of reverse bias. Now, different reverse biases are applied to the absorber section of the diode laser and corresponding characteristic curves are recorded. It is shown in Figure 5.12:

It can be seen from Figure 5.12 that with increasing reverse bias, the threshold increases slightly and also the slope of the curve decreases. Usually, the increased reverse bias sweeps out of the carriers from the absorber section quickly and shorten the optical pulses.

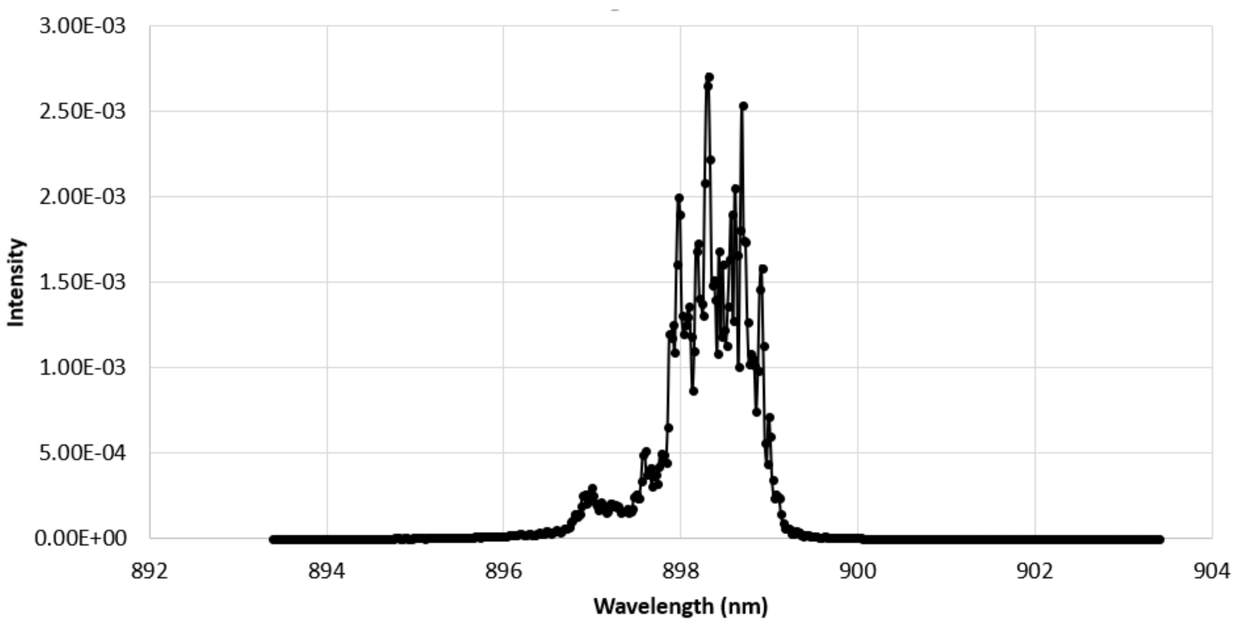

Figure 5.11: Optical spectrum of 2 section laser

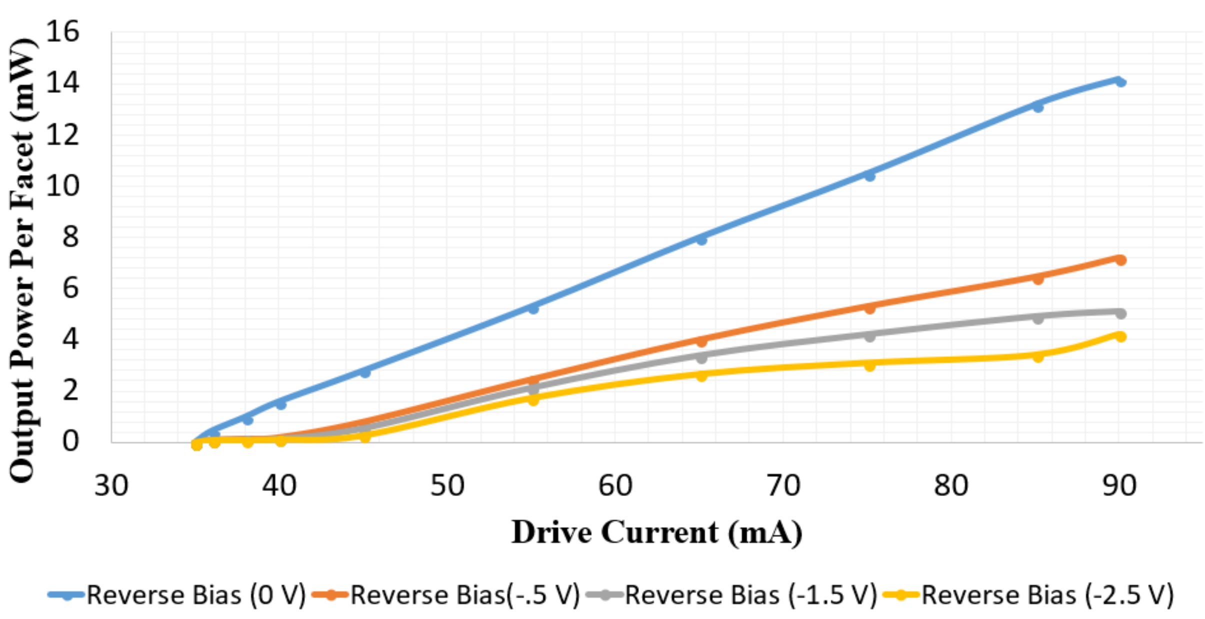

Figure 5.12: Impact of different reverse biases on passively mode locked laser

CHAPTER 6

CONCLUSION

This thesis aims to address different types of semiconductor lasers starting with broad area laser and followed by ridge waveguide laser and 2-section laser also known as passively mode-locked laser. It starts with the simulation of the diode lasers structures for figuring out the ridge height which will ensure fundamental mode lasing necessary condition for improving coupling of light into the optical fiber. FIMMWAVE software is utilized for this purpose. Detailed steps are explained here for fabrication of all these lasers. Related issues of the fabrication process and corresponding customized solutions are also explained here to overcome the issues. All the fabrication processes are carried out here in the clean room facility available at The University of Texas at Dallas.

The basic fabrication process includes photolithography, RCA cleaning, metal deposition, plasma enhanced chemical vapor deposition, plasma etching, and rapid thermal annealing. Once the fabrication is finished, samples are cleaved and characterized in the lab. The setup in the lab measures the light output along with emitted wavelength using the optical spectrum analyzer. Setup of the characterization is also explained in this thesis. Coupling of the output into the optical fiber is also explained here which is an important step in this process. However, coupling into single-mode fiber is found very daunting due to which further amplification is required before it can be used with autocorrelator. This autocorrelator will be used to characterize the short optical pulses. RF spectrum analyzer can be used also to see the spectrum.

It is found from the result section that the threshold current reduces significantly from 140 mA for broad area laser to around 26 mA for ridge waveguide laser. The measurement of EDQE shows that as the length of the cavity increases, the EDQE decreases. From this dependence, the inverse of the EDQE is plotted against the cavity length. The slope of the extrapolated line gives us the internal loss of 5.85 cm^{-1}. Also, the y intercept of this line gives us the IQE of 85.5%.The threshold current density is plotted against the inverse of the cavity length. To find the threshold current density of the diode laser for infinite length, the curve is extrapolated. It intercepts the y axis at 139.91. This value indicates that for infinite length the threshold current density will be 139.91 A/cm^2. The dependence of lasing threshold on the temperature is also shown here which indicates that as the temperature is increased, the threshold current increases along with decreased slope efficiency. Therefore, characteristic temperature is measured which measures the sensitivity of the diode laser. Higher value of characteristic temperature indicates that the diode laser will be more thermally stable. For the measured diode laser, the characteristic temperature is 208.3 ^0C.

The temperature not only impacts the threshold current but also the peak wavelength. Measurement shows that as the temperature is increased from 20 ^0C to 45 ^0C, the peak wavelength shifts from 897.22 nm to 905.16 nm. Finally, it is found that the threshold current for passively mode locked laser is higher compared to ridge waveguide laser. This can be attributed to the additional absorber section which is isolated from the gain section. Also, as the reverse bias is increased on the absorber section, the threshold current for the passively mode locked laser increases slightly along with reduced slope efficiency.

This thesis paves the way for future work of high frequency mode locking. The changing the length and the position of the absorber within the cavity, the type of mode locking and mode locking frequency can be changed. It is also possible to introduce passive sections at the end facets of the diode lasers which will prevent damage to the facets for high power lasers (Tandoi et al., 2012). In addition, semiconductor optical amplifiers can be defined at the end of gain sections to improve the output power. This demonstrates how from an individual diode laser, it is possible to incorporate other optical components like an amplifier, a modulator etc. to move towards photonic integrated circuits. I believe this thesis will be helpful to the people who will be willing to explore this exciting field of ultrafast optics.

REFERENCES

Achtenhagen, M., A. A. Hardy, and C. S. Harder (2006, May). Coherent kinks in high-power ridge waveguide laser diodes. *Journal of Lightwave Technology 24*(5), 2225–2232.

Afromowitz, M. A. (1974). Refractive index of $Ga_{1x}Al_xAs$. *Solid State Communications 15*(1), 59 – 63.

Agrawal, G. P. and N. K. Dutta (2013). *Semiconductor lasers*. Springer Science & Business Media.

Alferov, Z. I. (1969). AlAs-GaAs heterojunction injection lasers with a low room-temperature threshold. *Fiz, Tekh. Poluprov 3*, 1328–1332.

Basov, N., O. Krokhin, and Y. M. Popov (1961). Production of negative temperature states in pn junctions of degenerate semiconductors. *Sov. Phys. JETP 13*, 1320–1321.

Blood, P. (2015). *Quantum Confined Laser Devices: Optical gain and recombination in semiconductors*, Volume 23. OUP Oxford.

Camacho, F. (1998, February). Passive modelocking in semiconductor lasers with monolithically integrated passive waveguides. *IEE Proceedings - Optoelectronics 145*, 43–46(3).

Diehl, R. D. and R. L. Diehl (2000). *High-power diode lasers: fundamentals, technology, applications*, Volume 78. Springer Science & Business Media.

Ettenberg, M. (1975). Very lowthreshold doubleheterojunction $Al_xGa_{1-x}As$ injection lasers. *Applied Physics Letters 27*(12), 652–654.

Hall, R. N., G. E. Fenner, J. D. Kingsley, T. J. Soltys, and R. O. Carlson (1962, Nov). Coherent light emission from GaAs junctions. *Phys. Rev. Lett. 9*, 366–368.

Hou, L., E. A. Avrutin, R. Dylewicz, M. Haji, B. Qiu, and A. C. Bryce (2011, June). AlGaInAs mode-locked lasers for ultrashort pulse harmonic mode locking. In *2011 13th International Conference on Transparent Optical Networks*, pp. 1–4.

Keithly, M. (2002). Model 2520INT integrating sphere, quick start guide.

Marsh, J. H. and L. Hou (2017, Nov). Mode-locked laser diodes and their monolithic integration. *IEEE Journal of Selected Topics in Quantum Electronics 23*(6), 1–11.

Martins-Filho, J. F., E. A. Avrutin, C. N. Ironside, and J. S. Roberts (1995, Jun). Monolithic multiple colliding pulse mode-locked quantum-well lasers, experiment and theory. *IEEE Journal of Selected Topics in Quantum Electronics 1*(2), 539–551.

Mobarhan, K. S. (2018). Application note 1:Fiber optics and photonics, test and characterization of diode lasers: Determination of principal parameters.

Nathan, M. I., W. P. Dumke, G. Burns, F. H. Dill Jr, and G. Lasher (1962). Stimulated emission of radiation from GaAs p-n junctions. *Applied Physics Letters 1*(3), 62–64.

Nelson, H. and H. Kressel (1969). Improved red and infrared light emitting $Al_xGa_{1-x}As$ laser diodes using the close-confinement structure. *Applied Physics Letters 15*(1), 7–9.

Pusino, V. (2013, December). High power, high frequency mode-locked semiconductor lasers.

Pusino, V., M. J. Strain, and M. Sorel (2014, Dec). Passive mode-locking in semiconductor lasers with saturable absorbers bandgap shifted through quantum well intermixing. *Photon. Res. 2*(6), 186–189.

Qiu, B., S. D. McDougall, X. Liu, G. Bacchin, and J. H. Marsh (2005, Sept). Design and fabrication of low beam divergence and high kink-free power lasers. *IEEE Journal of Quantum Electronics 41*(9), 1124–1130.

Qiu, B. C., S. D. McDougall, X. F. Liu, G. Bacchin, and J. H. Marsh (2004, Nov). Design and fabrication of low beam divergence and high kink-free power 980 nm lasers. In *The 17th Annual Meeting of the IEEELasers and Electro-Optics Society, 2004. LEOS 2004.*, Volume 2, pp. 477–478 Vol.2.

Streetman, B. G. and S. K. Banerjee (2016). *Solid State Electronic Devices: Global Edition*. Pearson education.

Tandoi, G., C. N. Ironside, J. H. Marsh, and A. C. Bryce (2012, March). Output power limitations and improvements in passively mode locked GaAs/AlGaAs quantum well lasers. *IEEE Journal of Quantum Electronics 48*(3), 318–327.

Thorlabs, F. p. c. (July, 2018). http://www.thorlabs.com/.

Yanson, D. A., M. W. Street, S. D. McDougall, L. G. Thayne, J. H. Marsh, and E. A. Avrutin (2002, Jan). Ultrafast harmonic mode-locking of monolithic compound-cavity laser diodes incorporating photonic-bandgap reflectors. *IEEE Journal of Quantum Electronics 38*(1), 1–11.

BIOGRAPHICAL SKETCH

Banaful Paul, son of Mr. Balaram Paul and Mrs. Bandana Paul, was born on January 1st, 1989, in Chittagong, Bangladesh. He received his secondary and higher secondary education from Faujdarhat Cadet College in Chittagong, Bangladesh from 2001 to 2007. Later, he received his Bachelor of Science from Chittagong University of Engineering and Technology (CUET), Chittagong, Bangladesh in Electrical Engineering in 2012. Banaful Paul joined the The University of Texas at Dallas in January 2015 as a graduate student in the Electrical Engineering department. His research interests include semiconductor lasers and photonic integrated circuits.

CURRICULUM VITAE

Banaful Paul

Contact Information:

Email: banaful.paul2464@gmail.com

Educational History:

B.Sc., Electrical and Electronics Engineering, Chittagong University of Engineering and Technology, 2012

Employment History:

Lecturer, Chittagong University of Engineering and Technology, September 2013 – December 2014
Lecturer, Daffodil International University, January 2013 – May 2013

Research Experiences:

Fabrication and Characterization of GaAs/AlGaAs Broad Area Laser and Ridge Waveguide Laser
Theoretical study of mode locked diode lasers for improving monolithic integration of passive waveguide by Quantum Well Intermixing.
Fabrication and Characterization of Passively Mode Locked GaAs/AlGaAs Laser with low timing jitter for improved stability.
Application of TLM method to find out the contact resistance of P and N side contact layers of diode Laser.

Skills:

Experience in using commercial semiconductor device modelling software like R SOFT, LaserMOD, FIMMWAVE, PICWave, Harold.
Experience in Characterization of diode lasers using Optical Spectrum Analyzer (OSA), Autocorrelator, Beam Profiler and Integrating Sphere.
Experience in Photolithography at class 1000 cleanroom.
Experience in Reactive Ion Etching (RIE), Rapid Thermal Annealing (RTA), e-gun evaporator, PECVD, Wet and Dry etching and RCA cleaning.
Experience in using Optical Microscope, Atomic Force Microscopy (AFM), Profilometer.

Academic Awards

Prime Minister Gold Medal Award, 2012 (Highest GPA in the Faculty of Electrical & Computer Engineering)
University Gold Medal Award, 2012 (Highest GPA in the graduating batch)
Merit Award, 2011 (From Ex-Students association of CUET for academic excellence in the Dept. of EEE)